This is to certify that the

thesis entitled

Integral Equation Formulation for Natural Modes Of A Circular Patch Antenna In A Layered Environment

presented by

Eric William Blumbergs

has been accepted towards fulfillment
of the requirements for

Master's degree in EE

Dennis P. Nyquist
Major professor

Date July 17, 1989

INTEGRAL EQUATION FORMULATION FOR NATURAL MODES OF A CIRCULAR PATCH ANTENNA IN A LAYERED ENVIRONMENT

By

Eric William Blumbergs

A DISSERTATION

Submitted to
Michigan State University
in partial fulfillment of the requirements
for the degree of

MASTER OF SCIENCE

Department of Electrical Engineering

1989

ABSTRACT

INTEGRAL EQUATION FORMULATION FOR NATURAL MODES OF
A CIRCULAR PATCH ANTENNA IN A LAYERED ENVIRONMENT

By

Eric William Blumbergs

Conventional solutions yielding resonant frequencies of a circular patch antenna embedded in an integrated circuit environment utilize various approximations; thus, they produce reasonably accurate results for only a limited specification of physical parameters. A full wave analysis utilizing integral-operator techniques to determine the resonant characteristics of the patch circumvents this problem.

Using a polar coordinate Sommerfeld-integral representation of a Hertzian potential dyadic Green's function (which accommodates the possibility of surface wave excitation in the layered background) leads to coupled electric field integral equations (EFIE's) describing the circular disk. Resonant mode solutions satisfy the homogeneous specialization of these EFIE's.

For the lowest order resonant modes of the patch, the homogeneous equations decouple leading to independent IE's describing resonant modes supporting radial and circumferential currents. Numerical solutions for the resonant frequencies and current distributions of these modes are obtained via Galerkin's method.

ACKNOWLEDGEMENTS

Great appreciation and thanks are expressed to major professor Dennis P. Nyquist for his guidance, assistance and patience throughout this research. Thanks must also be expressed to Dr. Edward J. Rothwell and Dr. Kun-Mu Chen for their encouragement and support. I would also like to thank fellow student Michael Blischke for his generous assistance and advice.

Finally, I am grateful to my mother, Patricia Blumbergs, and my father, Peter Blumbergs, for their support and understanding throughout my graduate study.

TABLE OF CONTENTS

LIST OF FIGURES

CHAPTER I

INTRODUCTION

The birth of microwave integrated electronics has created a growing interest in the use of microwave patch devices as resonators or antennas. Obtaining accurate resonant frequencies for patch antennas is of importance, due to their narrow bandwidth rendering them ineffective outside the vicinity of their resonant frequencies. For the circular resonator many approximate methods have been explored, but yield accurate results for only a limited range of physical parameters. This dissertation provides a conceptually exact description of a circular conducting patch immersed in an integrated circuit environment.

Commonly, approximate methods of analysis for the circular patch have proceeded through a quasi-static approach relying on calculating the resonant frequencies from the fringing field capacitance. Most of the approximate methods often ignore or heuristically account for radiation damping. To accommodate a more rigorous formulation prompts application of integral-operator techniques. Recently, integral equation analysis of the circular patch involving Hankel transform techniques has been investigated [1-3].

This research exploits an integral-operator description of the circular patch. The text is divided into five chapters. Chapter two provides the EM theory relevant to the integrated circuit environment of interest. Once the necessary theory is presented, a general integral equation (IE) formulation for resonant structures within this

environment is developed. In chapter three, this IE formulation is applied to the circular patch, resulting in a pair of homogeneous coupled IE's describing resonant modes of the patch. For the simplest modes, chapter four illustrates how the IE's decouple. These decoupled IE's, describing angularly invariant modes of resonance, may be numerically solved via Galerkin's method.

Some clarification about notation and assumptions used throughout this dissertation may be useful. Vector and dyadic quantities appear boldface and are identified with arrows and double bar double arrows, respectively. Harmonic time dependence of $e^{+j\omega t}$ is assumed, but suppressed throughout (this sign convention becomes extremely important in making key observations later on). Finally, all media are linear, homogeneous and isotropic.

CHAPTER II

ANALYSIS OF A RESONANT STRUCTURE IN A LAYERED ENVIRONMENT

2.1 INTRODUCTION

This chapter investigates the resonance of an arbitrarily shaped conducting patch immersed in an integrated conductor/film/cover environment. Attention is focused on describing the natural resonance of the device via integral-operator techniques. Once the integral equation for the patch currents at resonance is obtained, the excitation amplitudes of the resonant currents and the order of the resonance are determined.

The geometry considered is depicted in Figure 1. A film layer of thickness t and permittivity ε_f is deposited over a perfectly conducting ground plane (y=-t). The space above the film (y>0) is occupied by a cover dielectric with permittivity ε_c. Within the flim/cover interface (y=0) exists the patch device of infinite conductivity. The unit vector $\hat{t}$, not to be confused with thickness, is tangential to the patch surface. Also, all materials are non-magnetic and infinite in extent.

In section 2.2, the electromagnetics of the layered environment mentioned above are reviewed. Description of the electric field in the cover region is expressed in terms of an electric type Hertz potential, $\vec{\Pi}(\vec{r})$, which is represented by the inner product of a necessary Green's dyad and an electric source current which sustains the field. The

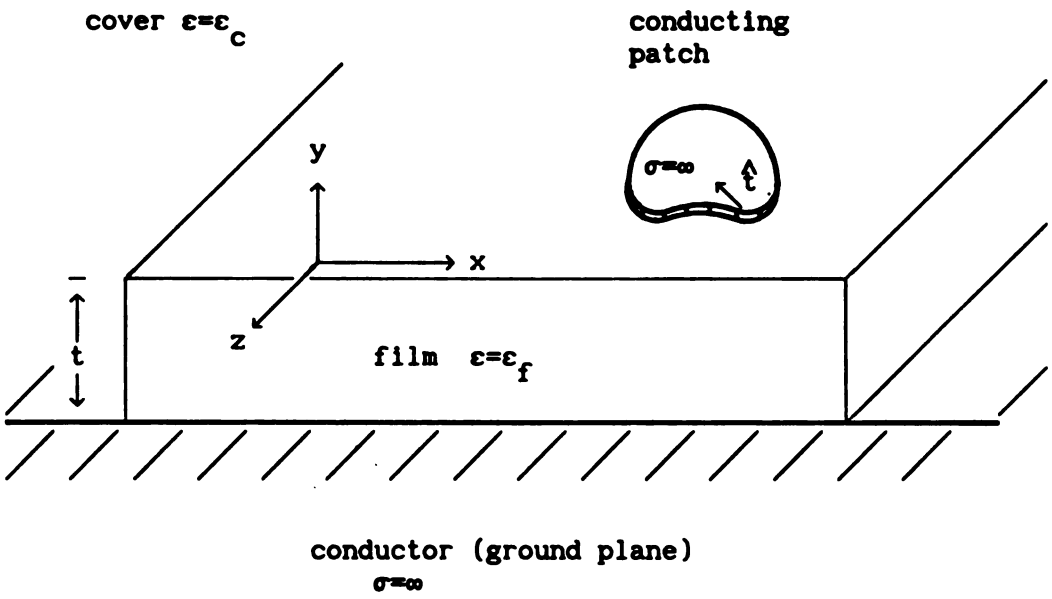

Figure 1. Arbitrarily shaped conducting patch immersed in the conductor/film/cover environment.

Green's dyad is expressed in terms of Sommerfeld-type integrals. The general development of a Green's dyad for tri-layered substrate/film-/cover dielectric media has been discussed by Nyquist and Bagby [4]. The dyad used in this analysis is the dyad discussed in [4], but specialized to a perfectly conducting substrate.

In the next section, the integral-operator description for the patch currents at resonance is pursued. The electric field in the cover, which consists of a scattered field due to surface currents on the patch and an impressed field exciting the patch, is expressed. Applying the necessary boundary condition at the patch surface leads to an electric field integral equation (EFIE), but a broader interpretation of this equation leads to an integral operator description of the resonant patch currents.

Finally, by carefully representing the current near resonance and making various other approximations on the EFIE mentioned previously, the order of the resonance and the corresponding current excitation amplitude coefficient may be obtained.

2.2 ELECTRIC FIELD IN THE COVER

This section presents the expressions for obtaining the electric field in the cover region of the conductor/film/cover environment. This electric field, as it will soon be seen, can be expressed in terms of a Hertz potential which, in turn, may be obtained through use of a dyadic Green's function. This dyad will be used extensively throughout Chapters II and III; thus, it requires a somewhat complete explanation. No details of the dyad's derivation will be given though. If knowledge of the derivation is desired, then reference [4] should be consulted.

The electric field maintained by an arbitrary current source in the cover region of the conductor/film/cover environment can be expressed in terms of an electric type Hertz potential [5] as

$$\vec{E}(\vec{r}) = (k_c^2 + \nabla\nabla\cdot)\vec{\Pi}(\vec{r}) \tag{1}$$

where $k_c^2 = \omega^2\mu\varepsilon_c$ and $k_c = +\omega\sqrt{\mu_o\varepsilon_c}$. The Hertz potential, $\vec{\Pi}(\vec{r})$, is expressed as

$$\vec{\Pi}(\vec{r}) = \int_{v'} \overleftrightarrow{G}(\vec{r}|\vec{r}\,') \cdot \frac{\vec{J}(\vec{r}\,')}{j\omega\varepsilon_c}\, dv' \tag{2}$$

where $\overleftrightarrow{G}(\vec{r}|\vec{r}\,')$ is the Hertzian potential Green's dyad for tri-layered dielectric media specialized to the conductor/film/cover environment, and $\vec{J}(\vec{r}\,')$ is the source present in the cover region.

The Green's dyad mentioned above consists of a principal and reflected dyad: $\overleftrightarrow{G}(\vec{r}|\vec{r}\,') = \overleftrightarrow{I}G^p(\vec{r}|\vec{r}\,') + \overleftrightarrow{G}^r(\vec{r}|\vec{r}\,')$. The principal dyad is represented by the unit dyad weighted by

$$G^p(\vec{r}|\vec{r}\,') = \int_{-\infty}^{\infty}\int \frac{e^{j\vec{\lambda}\cdot(\vec{r}-\vec{r}\,')}\, e^{-p_c|y-y'|}}{8\pi^2 p_c}\, d^2\lambda \tag{3}$$

which is the two dimensional inverse transform representation of the scalar Green's function in an unbounded cover,

$$G^p(\vec{r}|\vec{r}\,') = \frac{e^{-jk_c|\vec{r}-\vec{r}\,'|}}{4\pi|\vec{r}-\vec{r}\,'|}.$$

In eq. (3) the following relationships hold:

$$\lambda = \sqrt{\xi^2 + \zeta^2} \qquad d^2\lambda = d\xi d\zeta$$

$$\vec{\lambda} = \xi\hat{x} + \zeta\hat{z} \qquad p_c = \sqrt{\lambda^2 - k_c^2}\,.$$

In all the above relationships, subscript c denotes the cover region. Also, ξ and ζ are the 2-d transform variables. This portion of the Green's dyad corresponds to a primary wave of potential, $\vec{\Pi}^p(\vec{r})$, due to source currents embedded in an unbounded cover region.

The reflected dyad may be expressed as

$$\overleftrightarrow{G}^r(\vec{r}|\vec{r}') = \hat{x}G_t^r\hat{x} + \hat{y}\left[\frac{\partial}{\partial x}G_c^r\hat{x} + G_n^r\hat{y} + \frac{\partial}{\partial z}G_c^r\hat{z}\right] + \hat{z}G_t^r\hat{z}$$

where the various scalar components are given in inverse spectral form as

$$\begin{Bmatrix} G_t^r(\vec{r}|\vec{r}') \\ G_n^r(\vec{r}|\vec{r}') \\ G_c^r(\vec{r}|\vec{r}') \end{Bmatrix} = \iint_{-\infty}^{\infty} \begin{Bmatrix} R_t(\lambda) \\ R_n(\lambda) \\ C(\lambda) \end{Bmatrix} \frac{e^{j\vec{\lambda}\cdot(\vec{r}-\vec{r}')}\, e^{-p_c(y+y')}}{8\pi^2 p_c}\, d^2\lambda. \qquad (4)$$

$R_t(\lambda)$, $R_n(\lambda)$, the reflection coefficients, and $C(\lambda)$, the coupling coefficient, assume the following forms:

$$R_t(\lambda) = \frac{p_c - p_f\coth(p_f t)}{Z^h(\lambda)}$$

$$R_n(\lambda) = \frac{N_{fc}^2 p_c - p_f\tanh(p_f t)}{Z^e(\lambda)}$$

$$C(\lambda) = \frac{2(N_{fc}^2 - 1)p_c}{Z^h(\lambda)\, Z^e(\lambda)}$$

with

$$Z^h(\lambda) = p_c + p_f \coth(p_f t)$$

$$Z^e(\lambda) = N_{fc}^2 p_c + p_f \tanh(p_f t)$$

$$N_{fc} = \frac{n_f}{n_c} \quad \text{and} \quad p_\ell = \sqrt{\lambda^2 - k_\ell^2} \quad \text{for } \ell = c, f.$$

The subscript f denotes the flim region. Also, the relationships for the transform variable λ are identical to the ones used for the principal dyad. The quantities n_f and n_c represent the refractive indices of the film and cover, respectively.

This reflected dyad corresponds to a reflected wave of potential in the cover, which represents a sum of all waves reflected from the interface regions in Figure 1. It is important to observe that this reflected dyad is complicated by the coupling terms $\hat{y}\frac{\partial}{\partial x} G_c^r \hat{x}$ and $\hat{y}\frac{\partial}{\partial z} G_c^r \hat{z}$. Physically, these coupling terms correspond to normal components of reflected potential due to tangential components of polarization currents at the interface. Also, this reflected dyad accommodates the possibility of surface wave excitation in the layered surround. This phenomenon manifests itself in the terms $Z^h(\lambda)$ and $Z^e(\lambda)$ evident in the reflection and coupling coefficients described above. When these terms are identically zero (during inversion integration) they lead to pole singularities and represent the characteristic equations for TE odd and TM even surface waves in the layered surround.

2.3 INTEGRAL-OPERATOR DESCRIPTION OF RESONANT STRUCTURES

With the help of results presented in the last section, the objective of this section will be to obtain an integral-operator description of a resonant conducting patch immersed in the geometry previously described (see Figure 1). As mentioned previously, the patch is of arbitrary shape, is infinitely thin, and is perfectly conducting.

By properly expressing the fields in the cover region, an EFIE describing the patch can be constructed. The total electric field within the cover region may be expressed as $\vec{E}^t(\vec{r}) = \vec{E}^i(\vec{r}) + \vec{E}^s(\vec{r})$. The field component $\vec{E}^i(\vec{r})$ represents the impressed field exciting the patch (e.g., plane wave or microstrip line). The field component $\vec{E}^s(\vec{r})$ represents the scattered field maintained by induced surface currents on the conducting patch. This scattered field may be expressed by specializing eqs. (2.1) and (2.2) as

$$\vec{E}^s(\vec{r}) = -\frac{j\eta_c}{k_c}(k_c^2 + \nabla\nabla\cdot)\int_{s'} \overleftrightarrow{G}(\vec{r}|\vec{r}')\cdot\vec{K}(\vec{r}')\,ds' \tag{5}$$

where $$\frac{1}{j\omega\varepsilon_c} = -j\frac{1}{\omega\sqrt{\mu_o\varepsilon_c}}\sqrt{\frac{\mu_o}{\varepsilon_c}} = -j\frac{\eta_c}{k_c}.$$

Since the patch is perfectly conducting, the total tangential electric field on the patch surface must vanish. This condition may be stated as $\hat{t}\cdot\vec{E}^s(\vec{r}) = -\hat{t}\cdot\vec{E}^i(\vec{r})|_{\vec{r}\in s}$. Using expression (5), this boundary condition leads to the following EFIE:

$$\hat{t}\cdot(k_c^2 + \nabla\nabla\cdot)\int_{s'} \overleftrightarrow{G}(\vec{r}|\vec{r}')\cdot\vec{K}(\vec{r}')\,ds' = -j\frac{k_c}{\eta_c}\hat{t}\cdot\vec{E}^i(\vec{r}) \qquad \vec{r}\in s. \tag{6}$$

By making suitable modifications, an integral equation describing natural resonances of the patch can be extracted from eq. (6). First, for reasons that will quickly become evident, it is advantageous to use a broader interpretation of this equation leading to

$$\hat{t}\cdot(k_c^2 + \nabla\nabla\cdot)\int_{s'} \overleftrightarrow{G}(\vec{r}|\vec{r}',\omega)\cdot\vec{K}(\vec{r}',\omega)\,ds' = -j\frac{k_c}{\eta_c}\hat{t}\cdot\vec{E}^i(\vec{r},\omega) \qquad \vec{r}\in s \tag{7}$$

where $\overleftrightarrow{G}(\vec{r}|\vec{r}',\omega)$, $\vec{K}(\vec{r}',\omega)$, and $\vec{E}^i(\vec{r},\omega)$ are the temporal transform domain representations of $\overleftrightarrow{G}(\vec{r}|\vec{r}')$, $\vec{K}(\vec{r}')$, and $\vec{E}^i(\vec{r})$. Next, it may be assumed that temporal resonances of the patch correspond to pole singularities of $\vec{K}(\vec{r}',\omega)$ in the complex frequency domain. Thus, near resonance $\vec{K}(\vec{r}',\omega)$ may be expressed as

$$\vec{K}(\vec{r}',\omega) \cong a_p\frac{\vec{K}_p(\vec{r}')}{(\omega-\omega_p)^{\ell}} \tag{8}$$

where a_p is the excitation current amplitude, $(\omega-\omega_p)^{\ell}$ is the required pole singularity, and $\vec{K}_p(\vec{r}')$ is the normalized resonant surface current on the patch. For convenience, it is assumed the pole is of first order and the excitation current amplitude equals unity (the order of the pole singularity and the value of the excitation amplitude are considered in the next section); therefore, eq. (8) may be specialized as

$$\vec{K}(\vec{r}',\omega) = \frac{\vec{K}_p(\vec{r}')}{(\omega-\omega_p)}. \tag{9}$$

The motivation for representing the current in this manner becomes evident if it is substituted into eq. (7) and the limit as ω approaches ω_p is considered yielding

$$\lim_{\omega\to\omega_p} \frac{\hat{t}\cdot(k_c^2 + \nabla\nabla\cdot)}{\omega-\omega_p} \int_{s'} \overleftrightarrow{G}(\vec{r}|\vec{r}',\omega)\cdot\vec{K}_p(\vec{r}')ds'$$

$$= \lim_{\omega\to\omega_p} -j\frac{k_c}{\eta_c}\,\hat{t}\cdot\vec{E}^i(\vec{r},\omega) \qquad \vec{r}\in s. \tag{10}$$

From this EFIE, it can be seen that as ω approaches ω_p, the LHS of the equation becomes unbounded, while the RHS of the equation remains finite since $\vec{E}^i(\vec{r},\omega)$ is regular at $\omega=\omega_p$. Because this is impossible, the LHS of eq. (10) is forced to become an indeterminate form which finally leads to the desired equation for natural resonance of the patch device;

$$\hat{t}\cdot(k_c^2 + \nabla\nabla\cdot)\int_{s'} \overleftrightarrow{G}(\vec{r}|\vec{r}',\omega_p)\cdot\vec{K}_p(\vec{r}')ds' = 0 \qquad \vec{r}\in s. \tag{11}$$

2.4 EXCITATION OF RESONANT MODES

To accommodate the determination of ℓ (pole order) and a_p (excitation amplitude) evident in relation (8), EFIE (7) must be suitably expressed. First, by passing $(k_c^2 + \nabla\nabla\cdot)$ inside the integral, EFIE (7) may be rearranged as

$$\hat{t}\cdot\int_{s'}\overleftrightarrow{G}_e(\vec{r}|\vec{r}',\omega)\cdot\vec{K}(\vec{r}',\omega)\,ds' = -j\frac{k_c}{\eta_c}\,\hat{t}\cdot\vec{E}^i(\vec{r},\omega) \qquad \vec{r}\in s. \tag{12}$$

$\overleftrightarrow{G}_e(\vec{r}|\vec{r}',\omega)$, an electric Green's dyad [4,6], is expressed as

$$\overleftrightarrow{G}_e(\vec{r}|\vec{r}',\omega) = PV(k_c^2 + \nabla\nabla\cdot)\overleftrightarrow{G}(\vec{r}|\vec{r}',\omega) + \overleftrightarrow{L}\delta(\vec{r}-\vec{r}').$$

(PV indicates $\overleftrightarrow{G}_e$ is integrated in a principle volume sense [7] by excluding a "slice" principle volume [8] accommodating the source point singularity at y=y', and $\overleftrightarrow{L}=-\hat{y}\hat{y}$ is an associated depolarizing dyad [9].) Next, since $\vec{K}_p(\vec{r})$ (the p'th resonant current) is tangent to the patch, $\hat{t}\cdot$(argument) may be replaced on both sides of EFIE (12) with $\int_s\vec{K}_p(\vec{r})\cdot$(arg.)ds leading to

$$\int_s ds\int_{s'}\vec{K}_p(\vec{r})\cdot\overleftrightarrow{G}_e(\vec{r}|\vec{r}',\omega)\cdot\vec{K}(\vec{r}',\omega)\,ds' = -j\frac{k_c}{\eta_c}\int_s\vec{K}_p(\vec{r})\cdot\vec{E}^i(\vec{r},\omega)\,ds. \tag{13}$$

Finally, by using reciprocity of the electric Green's dyad [5], relation (13) may be rewritten as

$$\int_{s'}ds'\vec{K}(\vec{r}',\omega)\cdot\int_s\overleftrightarrow{G}_e(\vec{r}'|\vec{r},\omega)\cdot\vec{K}_p(\vec{r})\,ds = -j\frac{k_c}{\eta_c}\int_s\vec{K}_p(\vec{r})\cdot\vec{E}^i(\vec{r},\omega)\,ds. \tag{14}$$

Near resonance ($\omega\cong\omega_p$), modifications on expression (14) may be made which will inevitably lead to the desired knowledge of the pole order and the excitation coefficient. First, $\overleftrightarrow{G}_e(\vec{r}'|\vec{r},\omega)$ may be expanded in a Taylor series about the resonant frequency $\omega=\omega_p$ as

$$\overleftrightarrow{G}_e(\vec{r}'|\vec{r},\omega) \cong \overleftrightarrow{G}_e(\vec{r}'|\vec{r},\omega_p) + \frac{\partial}{\partial\omega}\overleftrightarrow{G}_e(\vec{r}'|\vec{r},\omega)\Big|_{\omega=\omega_p}(\omega-\omega_p) + \ldots \tag{15}$$

Also, as it was seen earlier, near resonance $\vec{K}(\vec{r}',\omega)$ can be represented by relation (8). Substituting these representations for $\vec{K}(\vec{r}',\omega)$ and $\overleftrightarrow{G}_e(\vec{r}'|\vec{r},\omega)$ into expression (14) and employing relation (11) yields

$$\frac{a_p}{(\omega-\omega_p)^{\ell}}\int_{s'} ds'\vec{K}_p(\vec{r}')\cdot\int_s\left[\frac{\partial}{\partial\omega}\overleftrightarrow{G}_e(\vec{r}'|\vec{r},\omega)\Big|_{\omega=\omega_p}(\omega-\omega_p) + \ldots\right]\cdot\vec{K}_p(\vec{r})\,ds$$

$$= -j\frac{k_c}{\eta_c}\int_s \vec{K}_p(\vec{r})\cdot\vec{E}^i(\vec{r},\omega)\,ds. \tag{16}$$

From eq. (16) it may be concluded that as long as

$$\int_{s'} ds'\vec{K}_p(\vec{r}')\cdot\int_s\left[\frac{\partial}{\partial\omega}\overleftrightarrow{G}_e(\vec{r}'|\vec{r},\omega)\Big|_{\omega=\omega_p}(\omega-\omega_p)\right]\cdot\vec{K}_p(\vec{r})\,ds \tag{17}$$

is non-vanishing, then ℓ=1 (first order pole) so that the apparent singularity on the LHS of this equation is annulled when ω approaches resonance. With ℓ determined, eq. (16) may be rearranged yielding the following expression for the excitation coefficient a_p

$$a_p = -\frac{jk_c}{\eta_c C_p}\int_s \vec{K}_p(\vec{r})\cdot\vec{E}^i(\vec{r},\omega)\,ds \qquad \text{where}$$

$$C_p = \int_{s'} ds'\vec{K}_p(\vec{r}')\cdot\int_s\left[\frac{\partial}{\partial\omega}\overleftrightarrow{G}_e(\vec{r}'|\vec{r},\omega)\Big|_{\omega=\omega_p}(\omega-\omega_p)\right]\cdot\vec{K}_p(\vec{r})\,ds.$$

It is important to note that the above expression for a_p is valid only

for ω near ω_p. Since, ω is real (the patch will most likely by excited by a driven element) and ω_p is complex, $\omega=\omega_p$ cannot occur (unless excitation is caused by an indentical resonating patch). Maximum patch excitation amplitude occurs when $\omega=\omega_{pr}$, and frequencies for which ω is distant from ω_{pr} (real part of ω_p) are unimportant because the resulting amplitude is small.

In the previous development, it was assumed the integral specified by eq. (17) was non-vanishing giving rise to a first order pole. If this leading term vanishes, integration of higher order terms evident in expression (15) into the patch surface current must be considered, giving rise to higher-ordered poles.

2.5 Summary

In the tri-layered conductor/film/cover environment, the scattered electric field in the cover maintained by currents excited on a perfectly conducting, infinitely-thin patch resonator of arbitrary shape embedded in the film/cover interface may be expressed as

$$\vec{E}^s(\vec{r}) = -j \frac{\eta_c}{k_c} (k_c^2 + \nabla\nabla\cdot) \int_{s'} \overleftrightarrow{G}(\vec{r}|\vec{r}') \cdot \vec{K}(\vec{r}') \, ds'. \tag{2.5}$$

$\overleftrightarrow{G}(\vec{r}|\vec{r}')$, the Hertzian potential Green's dyad, consists of a principal and reflected dyad: $\overleftrightarrow{G}(\vec{r}|\vec{r}') = \overleftrightarrow{I}G^p(\vec{r}|\vec{r}') + \overleftrightarrow{G}^r(\vec{r}|\vec{r}')$. The principal dyad corresponds to a primary wave of potential due to currents embedded in a hypothetical unbounded cover. The reflected dyad corresponds to a reflected wave of potential due to polarization currents excited at the film/cover and conductor/film interfaces.

By applying the appropriate boundary conditions at the patch surface and exploiting relation (2.5), the following EFIE can be constructed:

$$\hat{t}\cdot(k_c^2 + \nabla\nabla\cdot)\int_{s'} \overleftrightarrow{G}(\vec{r}|\vec{r}',\omega)\cdot\vec{K}(\vec{r}',\omega)\, ds' = -j\frac{k_c}{\eta_c}\hat{t}\cdot\vec{E}^i(\vec{r},\omega) \qquad \vec{r}\in s. \quad (2.7)$$

Using reasonable assumptions near resonance allows $\vec{K}(\vec{r}',\omega)$ to be represented as

$$\vec{K}(\vec{r}',\omega) \cong a_p \frac{\vec{K}_p(\vec{r}')}{(\omega-\omega_p)^{\ell}} . \quad (2.8)$$

Properly using this representation in EFIE (2.7) leads to

$$\hat{t}\cdot(k_c^2 + \nabla\nabla\cdot)\int_{s'} \overleftrightarrow{G}(\vec{r}|\vec{r}',\omega_p)\cdot\vec{K}_p(\vec{r}')ds' = 0 \qquad \vec{r}\in s. \quad (2.11)$$

The above expression may be interpreted as an integral equation which describes natural resonance of the patch device.

An expression for a_p and the value of ℓ (order of resonance) in relation (2.8) can be obtained by rearranging EFIE (2.7) as

$$\hat{t}\cdot\int_{s'} \overleftrightarrow{G}_e(\vec{r}|\vec{r}',\omega)\cdot\vec{K}(\vec{r}',\omega)\, ds' = -j\frac{k_c}{\eta_c}\hat{t}\cdot\vec{E}^i(\vec{r},\omega) \qquad \vec{r}\in s \quad (2.12)$$

where $\overleftrightarrow{G}_e(\vec{r}|\vec{r}',\omega)$ now represents an electric Green's dyad. By substituting relation (2.8) into EFIE (2.12), applying reciprocity, and expanding $\overleftrightarrow{G}_e(\vec{r}'|\vec{r},\omega)$ in a Taylor series about the resonant frequency ω_p, the value

of ℓ can be deduced and an expression for a_p can be obtained. For the case ℓ=1, a_p was found to be

$$a_p = - \frac{jk_c}{\eta_c C_p} \int_s \vec{K}_p(\vec{r}) \cdot \vec{E}^i(\vec{r}, \omega_e) \, ds \qquad \text{where}$$

$$C_p = \int_{s'} ds' \vec{K}_p(\vec{r}') \cdot \int_s \left[\frac{\partial}{\partial \omega} \overleftrightarrow{G}_e(\vec{r}' | \vec{r}, \omega) \Big|_{\omega=\omega_p} \right] \cdot \vec{K}_p(\vec{r}) \, ds.$$

CHAPTER III

DETAILED ANALYSIS OF A CIRCULAR PATCH

3.1 INTRODUCTION

The last chapter investigated resonance of an arbitrarily shaped conducting patch in a tri-layered environment. The chapter at hand focuses attention on a specific structure in the same environment, namely, a circular patch. The goal is to obtain an integral-operator description of the patch at resonance. The procedure is similar to the one demonstrated in section 2.3, but more details are carried out since a specific geometry is implied.

Since the resonant structure has circular symmetry, the rectangular component Green's dyad of section 2.2 is transformed to polar form. First, the Sommerfeld integrals of the scalar component Green's functions are converted to the appropriate cylindrical coordinates. Then, the unit vectors of the dyad are transformed.

In section 3.3, the polar component Hertzian potential is obtained. Because the patch has circular symmetry, the radial and the circumferential components of surface current on the patch (K_ρ and K_θ) may be expanded in an angular Fourier series. Integration of these current components into the polar Green's dyad yields the desired expression for the Hertzian potential in the cover.

Finally, by using the Hertzian potential, the electric field in the cover, maintained by the patch surface currents, is constructed. With

the use of this field, the desired polar component integral equations for the patch currents at resonance may be derived.

3.2 POLAR COMPONENT GREEN'S DYAD

The rectangular component Green's dyad of section 2.2 can alternatively be represented in the following spatial and spectral polar coordinates:

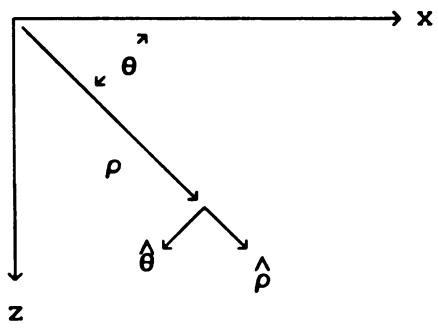

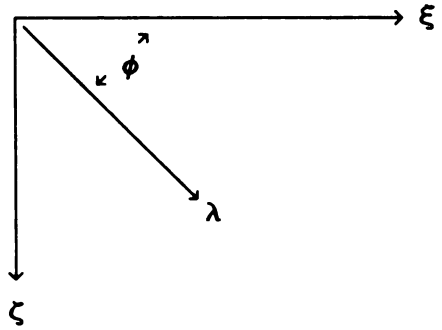

$x = \rho\cos\theta$
$z = \rho\sin\theta$
$\hat{\rho} = \hat{x}\cos\theta + \hat{z}\sin\theta$
$\hat{\theta} = -\hat{x}\sin\theta + \hat{z}\cos\theta$

$\xi = \lambda\cos\phi$
$\zeta = \lambda\sin\phi$
$d\xi d\zeta = \lambda d\lambda d\phi$

Considering first the spectral integral representations of the scalar components of $\overleftrightarrow{G}(\vec{r}|\vec{r}')$ (eqs. (2.3) and (2.4)), it is seen they take the followings generic form

$$I(\vec{r}|\vec{r}') = \int_{-\infty}^{\infty}\int f(\lambda, y|y')e^{j\vec{\lambda}\cdot(\vec{r}-\vec{r}')}\, d\xi d\zeta.$$

Geometrically, from the figure depicted on the next page it is obvious that $\vec{\lambda}\cdot(\vec{r}-\vec{r}')$ can equivalently be represented as $\lambda|\vec{\rho}-\vec{\rho}'|\cos(\phi-\psi)$.

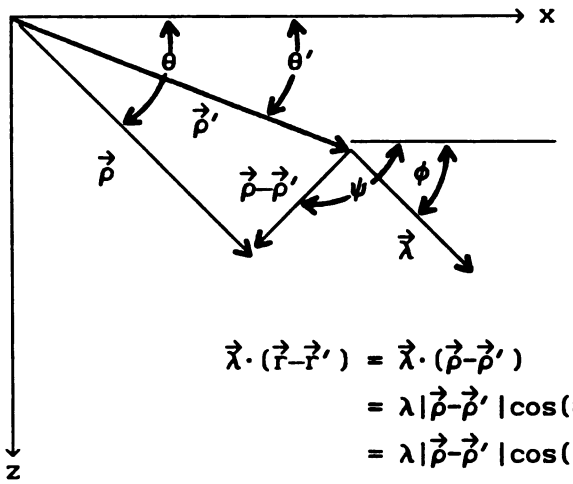

$$\vec{\lambda}\cdot(\vec{r}-\vec{r}') = \vec{\lambda}\cdot(\vec{\rho}-\vec{\rho}')$$
$$= \lambda|\vec{\rho}-\vec{\rho}'|\cos(\psi-\phi)$$
$$= \lambda|\vec{\rho}-\vec{\rho}'|\cos(\phi-\psi)$$

By applying this result, $I(\vec{r}|\vec{r}')$ may be rewritten as

$$I(\vec{r}|\vec{r}') = \int_0^{\infty} \lambda d\lambda\ f(\lambda, y|y') \int_{-\pi}^{\pi} e^{j\lambda|\vec{\rho}-\vec{\rho}'|\cos(\phi-\psi)}\ d\phi.$$

This might seem to be the desired polar representation for the generic integral, but with some simple manipulations a more elegant form is obtainable. Utilizing the substitution $u=\phi-\psi$ and noting the evenness in the exponential allows $I(\vec{r}|\vec{r}')$ to become

$$I(\vec{r}|\vec{r}') = \int_0^{\infty} \lambda d\lambda\ f(\lambda, y|y')2\int_0^{\pi} e^{j\lambda|\vec{\rho}-\vec{\rho}'|\cos(u)}\ du.$$

Further, employing the integral representation of $J_o(x)$, the zeroth order Bessel function of the first kind [10], allows $I(\vec{r}|\vec{r}')$ to ultimately become

$$I(\vec{r}|\vec{r}') = 2\pi\int_0^\infty f(\lambda, y|y')J_o(\lambda|\vec{\rho}-\vec{\rho}'|)\ \lambda d\lambda \tag{1}$$

which is the desired polar representation. Thus, utilizing eq. (1) enables the spectral integrals in eqs. (2.3) and (2.4) to be expressed in polar form as

$$G^p(\vec{r}|\vec{r}') = \int_0^\infty \frac{J_o(\lambda|\vec{\rho}-\vec{\rho}'|)\ e^{-p_c|y-y'|}}{4\pi p_c}\ \lambda d\lambda \tag{2a}$$

$$\begin{Bmatrix} G_t^r(\vec{r}|\vec{r}') \\ G_n^r(\vec{r}|\vec{r}') \\ G_c^r(\vec{r}|\vec{r}') \end{Bmatrix} = \int_0^\infty \begin{Bmatrix} R_t(\lambda) \\ R_n(\lambda) \\ C(\lambda) \end{Bmatrix} \frac{J_o(\lambda|\vec{\rho}-\vec{\rho}'|)\ e^{-p_c(y+y')}}{4\pi p_c}\ \lambda d\lambda \tag{2b}$$

which completes the first portion of the polar transformation.

To finish the transformation, the components of the rectangular Green's dyad (e.g. $\hat{x}G_{xx}\hat{x}$, $\hat{y}G_{yz}\hat{z}$) must be converted to their appropriate polar representation (e.g. $\hat{\rho}G_{\rho\rho}\hat{\rho}$, $\hat{y}G_{y\theta}\hat{\theta}$). This is most easily accomplished by carrying out the dot product operations given by $G_{\alpha\nu} = \hat{\alpha}\cdot\overleftrightarrow{G}\cdot\hat{\nu}$, where α represents the field point components at ρ, θ, and y, and ν represents source point components at ρ',θ', and y'. Before this is done though, it is advantageous to rewrite the rectangular dyad of section 2.2, given as

$$\overleftrightarrow{G}(\vec{r}|\vec{r}') = \overleftrightarrow{I}G^p + \hat{x}G_t^r\hat{x} + \hat{y}\left[\frac{\partial}{\partial x}G_c^r\hat{x} + G_n^r\hat{y} + \frac{\partial}{\partial z}G_c^r\hat{z}\right] + \hat{z}G_t^r\hat{z}$$

in a more applicable form. This is accomplished by noting that the

partial derivatives operating on G_c in the yx and yz components of the dyad, are identically equivalent to the transverse gradient operating on G_c. With this observation in mind, $\overleftrightarrow{G}(\vec{r}|\vec{r}')$ may be rewritten as

$$\overleftrightarrow{G}(\vec{r}|\vec{r}') = \overleftrightarrow{I}G^p + \hat{x}G_t^r\hat{x} + \hat{y}\left[G_n^r\hat{y} + \nabla_t G_c^r\right] + \hat{z}G_t^r\hat{z}.$$

Also, noting that G_c^r is a function only of $|\vec{\rho}-\vec{\rho}'|$ enables ∇_t to be replaced by $-\nabla_t'$; therefore, the dyad may alternatively be expressed as

$$\overleftrightarrow{G}(\vec{r}|\vec{r}') = \overleftrightarrow{I}G^p + \hat{x}G_t^r\hat{x} + \hat{y}\left[G_n^r\hat{y} - \nabla_t' G_c^r\right] + \hat{z}G_t^r\hat{z}.$$

With $\overleftrightarrow{G}(\vec{r}|\vec{r}')$ expressed in this form, the dot products of $\overleftrightarrow{G}(\vec{r}|\vec{r}')\cdot\hat{v}$ may be easily calculated as

$$\overleftrightarrow{G}(\vec{r}|\vec{r}')\cdot\hat{\rho}' = \hat{x}(G^p+G_t^r)\cos\theta' - \hat{y}\,\frac{\partial}{\partial\rho'}\,G_c^r + \hat{z}(G^p+G_t^r)\sin\theta'$$

$$\overleftrightarrow{G}(\vec{r}|\vec{r}')\cdot\hat{\theta}' = -\hat{x}(G^p+G_t^r)\sin\theta' - \hat{y}\,\frac{1}{\rho'}\frac{\partial}{\partial\theta'}\,G_c^r + \hat{z}(G^p+G_t^r)\cos\theta'$$

$$\overleftrightarrow{G}(\vec{r}|\vec{r}')\cdot\hat{y}' = \hat{y}(G^p+G_n^r).$$

Continuing on with the dot products of $\hat{\rho}$, $\hat{\theta}$, and $\hat{y}$ into each of the above yields

$$\hat{\rho}\cdot\overleftrightarrow{G}(\vec{r}|\vec{r}')\cdot\hat{\rho}' = (G^p+G_t^r)\cos(\theta-\theta') \qquad \hat{\theta}\cdot\overleftrightarrow{G}(\vec{r}|\vec{r}')\cdot\hat{y}' = 0$$

$$\hat{\rho}\cdot\overleftrightarrow{G}(\vec{r}|\vec{r}')\cdot\hat{\theta}' = (G^p+G_t^r)\sin(\theta-\theta') \qquad \hat{y}\cdot\overleftrightarrow{G}(\vec{r}|\vec{r}')\cdot\hat{\rho}' = -\frac{\partial}{\partial\rho'}\,G_c^r$$

$$\hat{\rho}\cdot\overleftrightarrow{G}(\vec{r}|\vec{r}')\cdot\hat{y}' = 0 \qquad \hat{y}\cdot\overleftrightarrow{G}(\vec{r}|\vec{r}')\cdot\hat{\theta}' = -\frac{1}{\rho'}\frac{\partial}{\partial\theta'}\,G_c^r$$

$$\hat{\theta}\cdot\overleftrightarrow{G}(\vec{r}|\vec{r}')\cdot\hat{\rho}' = -(G^p+G_t^r)\sin(\theta-\theta') \qquad \hat{y}\cdot\overleftrightarrow{G}(\vec{r}|\vec{r}')\cdot\hat{y}' = G^p+G_n^r$$

$$\hat{\theta}\cdot\overleftrightarrow{G}(\vec{r}|\vec{r}')\cdot\hat{\theta}' = (G^p+G_t^r)\cos(\theta-\theta')$$

which completes the transformation of the unit vectors.

Finally, by using the above results along with expressions (2a) and (2b), the Green's dyad may be represented in polar form as

$$\overleftrightarrow{G}(\vec{r}|\vec{r}') = \begin{bmatrix} G_{\rho\rho} & G_{\rho\theta} & G_{\rho y} \\ G_{\theta\rho} & G_{\theta\theta} & G_{\theta y} \\ G_{y\rho} & G_{y\theta} & G_{yy} \end{bmatrix} \qquad \text{where}$$

$$G_{\rho\rho} = G_t\cos(\theta-\theta') \qquad G_{\rho\theta} = G_t\sin(\theta-\theta') \qquad G_{\rho y} = 0$$

$$G_{\theta\rho} = -G_t\sin(\theta-\theta') \qquad G_{\theta\theta} = G_t\cos(\theta-\theta') \qquad G_{\theta y} = 0$$

$$G_{y\rho} = -\frac{\partial}{\partial\rho'}G_c \qquad G_{y\theta} = -\frac{1}{\rho'}\frac{\partial}{\partial\theta'}G_c \qquad G_{yy} = G_n$$

where $G_t=G^p+G_t^r$, $G_n=G^p+G_n^r$, and $G_c=G_c^r$. With $\overleftrightarrow{G}(\vec{r}|\vec{r}')$ in this form it may now be applied to an appropriate situation, namely, a circular patch immersed in the conductor/film/cover environment. This will be the topic of section 3.3.

3.3 SPECIALIZATION TO A CIRCULAR PATCH

The geometry to be analyzed from here on is depicted in Figure 2. Figure 2 is a top view of Figure 1 with the arbitrarily shaped patch replaced by a circular patch, and the origin of coordinates shifted to the center of the circular patch. The circular patch has radius *a*, is

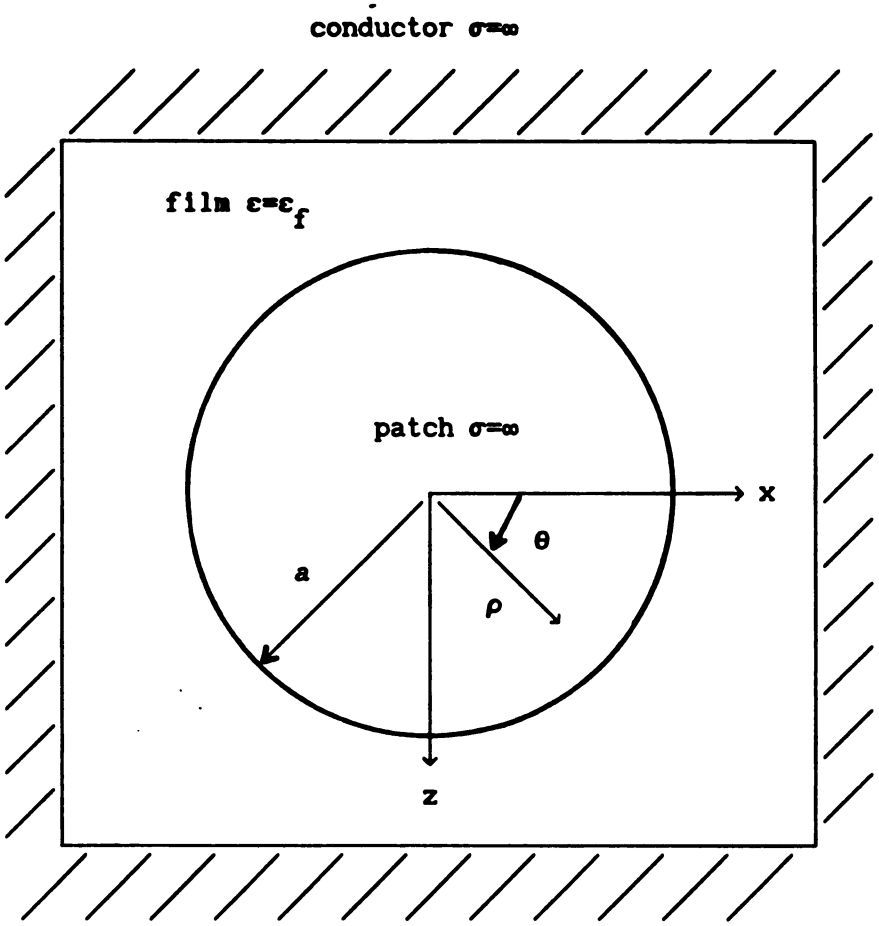

Figure 2. Geometry of circular patch (top view).

perfectly conducting, and infinitely thin. The patch resides in the film/cover interface (y=0). The polar coordinates for the patch are identical to the polar coordinates used in section 3.2 and the same relations hold.

Before determining the electric field in the cover due to the patch currents, it is desirable to obtain the Hertz potential in the simplest form possible. Taking advantage of the circular symmetry allows the current to be suitably modified, in turn, enabling the angular integrals in the Hertz potential to be analytically handled. Once the Hertz potential is in desirable form, the electric field induced by the radiating patch may be obtained, leading to the polar component IE's for the resonant patch currents.

3.3.1 HERTZ POTENTIAL IN THE COVER

In general, the Hertzian potential maintained in the cover region by an infinitely thin conducting patch immersed in the flim/cover interface may be written as

$$\vec{\Pi}(\vec{r}) = \frac{1}{j\omega\varepsilon_c} \int_{s'} \overset{\leftrightarrow}{G}(\vec{r}|\vec{r}') \cdot \vec{K}(\vec{r}')\, ds'. \tag{3}$$

For the situation about to be analyzed, though, it is most advantageous to represent the surface current as $\vec{K}(\vec{r}') = K_\rho(\rho',\theta')\hat{\rho}' + K(\rho',\theta')\hat{\theta}'$ and use the polar Green's dyad found in section 3.2 to express eq. (3) as

$$\Pi_\rho(\vec{r}) = \frac{1}{j\omega\varepsilon_c} \int_{s'} \Big[K_\rho(\rho',\theta')\cos(\theta-\theta') + K_\theta(\rho',\theta')\sin(\theta-\theta')\Big] G_t\, ds' \tag{4a}$$

$$\Pi_\theta(\vec{r}) = \frac{1}{j\omega\varepsilon_c}\int_{s'}\left[-K_\rho(\rho',\theta')\sin(\theta-\theta') + K_\theta(\rho',\theta')\cos(\theta-\theta')\right]G_t\ ds' \quad (4b)$$

$$\Pi_y(\vec{r}) = \frac{1}{j\omega\varepsilon_c}\int_{s'}\left[-K_\rho(\rho',\theta')\frac{\partial}{\partial\rho'} - K_\theta(\rho',\theta')\frac{1}{\rho'}\frac{\partial}{\partial\theta'}\right]G_c\ ds'. \quad (4c)$$

These representations for the various components of $\vec{\Pi}(\vec{r})$ are now in a form applicable to a circular patch.

From eqs. (4a), (4b), and (4c) it is obvious that little may be done to simplify these expressions until more is known about the behavior of the patch surface current. Noting the patch geometry, though, prompts the following rationale: the patch has circular symmetry; therefore, the current will be 2π periodic in θ and the various components of the surface current may be represented in an angular Fourier series expansion as

$$K_\alpha(\vec{\rho}') = \sum_{n=-\infty}^{\infty} A_{\alpha n}(\rho')e^{jn\theta'}. \quad (5)$$

If relation (5) is used for the various current components, eqs. (4a), (4b), and (4c) may be expressed as

$$\begin{matrix}\Pi_\rho \\ \theta\end{matrix} = \frac{1}{j\omega\varepsilon_c}\sum_n\int_0^a d\rho'\rho'\left[\pm A_{\rho n}(\rho')\int_{-\pi}^{\pi} e^{jn\theta'}\begin{Bmatrix}\cos(\theta-\theta') \\ \sin(\theta-\theta')\end{Bmatrix} G_t\ d\theta'\right.$$

$$\left. + A_{\theta n}(\rho')\int_{-\pi}^{\pi} e^{jn\theta'}\begin{Bmatrix}\sin(\theta-\theta') \\ \cos(\theta-\theta')\end{Bmatrix} G_t\ d\theta'\right] \quad (6a)$$

$$\Pi_y = \frac{1}{j\omega\varepsilon_c} \sum_n \int_0^a d\rho' \rho' \left[-A_{\rho n}(\rho') \frac{\partial}{\partial \rho'} + A_{\theta n}(\rho') \frac{1}{\rho'} \frac{\partial}{\partial \theta} \right] \int_{-\pi}^{\pi} e^{jn\theta'} G_c \, d\theta' . \qquad (6b)$$

In expression (6b) it is noted that $\frac{\partial}{\partial \theta'} \rightarrow - \frac{\partial}{\partial \theta}$ since G_c is only a function of $(\theta-\theta')$; thus, $\frac{\partial}{\partial \theta}$ may be brought outside the integral with respect to θ'.

Accounting for the azimuthal variation of the surface current, as illustrated in relation (5), allows for the analytic evaluation of the angular integrals evident in eqs. (6a) and (6b). Considering these integrals, it is evident that they assume the following forms:

$$I_1(\rho,\theta,\rho' | y,y') = \int_{-\pi}^{\pi} e^{jn\theta'} \begin{Bmatrix} \cos(\theta-\theta') \\ \sin(\theta-\theta') \end{Bmatrix} G_t(\rho,\rho';\theta-\theta' | y,y') \, d\theta'$$

$$I_2(\rho,\theta,\rho' | y,y') = \int_{-\pi}^{\pi} e^{jn\theta'} G_c(\rho,\rho';\theta-\theta' | y,y') \, d\theta' .$$

By making the substitution $u=\theta-\theta'$, and using the integral representations for G_t and G_c, I_1 and I_2 may be expressed as

$$I_1 = e^{jn\theta} \int_0^{\infty} \lambda d\lambda \, \frac{e^{-p_c|y-y'|} + R_t(\lambda) e^{-p_c(y+y')}}{4\pi p_c} \int_{-\pi}^{\pi} e^{-jnu} \begin{Bmatrix} \cos(u) \\ \sin(u) \end{Bmatrix} J_o(\lambda|\rho-\rho'|) \, du$$

$$I_2 = e^{jn\theta} \int_0^{\infty} \lambda d\lambda \, \frac{C(\lambda) e^{-p_c(y+y')}}{4\pi p_c} \int_{-\pi}^{\pi} e^{-jnu} J_o(\lambda|\vec{\rho}-\vec{\rho}'|) \, du$$

where $|\vec{\rho}-\vec{\rho}'| = \sqrt{\rho^2 + \rho'^2 - 2\rho\rho'\cos(u)}$.

The evaluation of the finite angular integrals in the previous expressions for I_1 and I_2 reduces to the evaluation of

$$f_n^{\substack{c\\s}}(\rho,\rho';\lambda) = \int_{-\pi}^{\pi} e^{-jnu} \begin{Bmatrix}\cos(u)\\ \sin(u)\end{Bmatrix} J_o(\lambda|\vec{\rho}-\vec{\rho}'|)\, du \tag{7a}$$

$$f_n^{e}(\rho,\rho';\lambda) = \int_{-\pi}^{\pi} e^{-jnu} J_o(\lambda|\vec{\rho}-\vec{\rho}'|)\, du \tag{7b}$$

where the superscripts c, s and e denote cosine, sine and empty (no cosine or sine), respectively. These evaluations can be readily achieved by using the summation theorem for J_o (see Appendix A). Applying this theorem first to eq. (7b) allows f_n^e to be rewritten as

$$f_n^e = \int_{-\pi}^{\pi} e^{-jnu} J_o(\lambda\sqrt{\rho^2 + \rho'^2 - 2\rho\rho'\cos(u)})\, du$$

$$= J_o(\lambda\rho)J_o(\lambda\rho')\int_{-\pi}^{\pi} e^{-jnu}\, du + 2\sum_{k=1}^{\infty} J_k(\lambda\rho)J_k(\lambda\rho')\int_{-\pi}^{\pi} e^{-jnu}\cos(ku)\, du. \tag{8}$$

From eq. (8) it can be seen that the only contribution from the first term occurs when n=0, yielding

$$J_o(\lambda\rho)J_o(\lambda\rho')\int_{-\pi}^{\pi} e^{-jnu}\, du = 2\pi J_o(\lambda\rho)J_o(\lambda\rho') \quad \text{for } n = 0$$

and due to orthogonality, the only contribution from the second term occurs when n=±k, yielding

$$2\sum_{k=1}^{\infty} J_k(\lambda\rho)J_k(\lambda\rho')\int_{-\pi}^{\pi} e^{-jnu}\cos(ku)\,du = 2\pi J_n(\lambda\rho)J_n(\lambda\rho') \quad \text{for } n = \pm1, \pm2, \ldots$$

Thus, f_n^e may be evaluated as

$$f_n^e = 2\pi J_n(\lambda\rho)J_n(\lambda\rho') \quad \text{for } n = 0, \pm1, \pm2, \ldots \tag{9}$$

By applying this result, eq. (7a), which with help of Euler's identity can be expressed as

$$f_n^{\substack{c\\s}} = \frac{1}{2}\int_{-\pi}^{\pi} \begin{Bmatrix} 1 \\ -j \end{Bmatrix} (e^{-j(n-1)u} \pm e^{-j(n+1)u})J_o(\lambda|\rho-\rho'|)\,du$$

may also be evaluated as

$$f_n^{\substack{c\\s}} = \begin{Bmatrix} 1 \\ -j \end{Bmatrix} \pi\Big[J_{n-1}(\lambda\rho)J_{n-1}(\lambda\rho') \pm J_{n+1}(\lambda\rho)J_{n+1}(\lambda\rho')\Big] \quad \text{for } n = 0, \pm1, \ldots \tag{10}$$

Finally, I_1 and I_2 may be expressed as

$$I_1 = e^{jn\theta}\, g_n^{\substack{c\\s}}(\rho, \rho' | y, y')$$

$$I_2 = e^{jn\theta}\, g_n^{e}(\rho, \rho' | y, y')$$

where

$$g_n^{c_s}(\rho,\rho'|y,y') = \int_0^\infty \lambda \frac{e^{-p_c|y-y'|} + R_t(\lambda)\, e^{-p_c(y+y')}}{4\pi p_c} f_n^{c_s}(\rho,\rho';\lambda)\, d\lambda \qquad (11)$$

$$g_n^{e}(\rho,\rho'|y,y') = \int_0^\infty \lambda \frac{C(\lambda)\, e^{-p_c(y+y')}}{4\pi p_c} f_n^{e}(\rho,\rho';\lambda)\, d\lambda \qquad (12)$$

with $f_n^{c_s}$ and f_n^{e} expressed in eqs. (9) and (10).

Applying the results obtained for I_1 and I_2, the polar components of the Hertz potential (eqs. (6a) and (6b)) become

$$\Pi_\rho(\vec{r}) = \frac{1}{j\omega\varepsilon_c} \sum_{n=-\infty}^{\infty} e^{jn\theta} \int_0^a \rho' \left[A_{\rho n}(\rho')\, g_n^c + A_{\theta n}(\rho')\, g_n^s\right] d\rho' \qquad (13)$$

$$\Pi_\theta(\vec{r}) = \frac{1}{j\omega\varepsilon_c} \sum_{n=-\infty}^{\infty} e^{jn\theta} \int_0^a \rho' \left[-A_{\rho n}(\rho')\, g_n^s + A_{\theta n}(\rho')\, g_n^c\right] d\rho' \qquad (14)$$

$$\Pi_y(\vec{r}) = \frac{1}{j\omega\varepsilon_c} \sum_{n=-\infty}^{\infty} e^{jn\theta} \int_0^a \rho' \left[-A_{\rho n}(\rho')\, \frac{\partial}{\partial\rho'}\, g_n^e + A_{\theta n}(\rho')\, \frac{jn}{\rho'}\, g_n^e\right] d\rho'. \qquad (15)$$

(The differentiation with respect to θ evident in eq. (6b) was evaluated in obtaining relation (15), leading to the jn term.) With the Hertzian potential in this relatively simplified form, the electric field in the cover and inevitably the resonant IE's for the circular patch can determined, as will be seen in section 3.3.2.

3.3.2 COUPLED POLAR COMPONENT RESONANT IE'S

The electric field components E_ρ^s and E_θ^s, maintained in the cover region by the patch surface currents, may be recovered using the results of section 3.3.1 along with the relations

$$E_\rho^s(\vec{r}) = k_c^2 \, \Pi_\rho(\vec{r}) + \frac{\partial}{\partial \rho} \nabla \cdot \vec{\Pi}(\vec{r}) \tag{16}$$

$$E_\theta^s(\vec{r}) = k_c^2 \, \Pi_\theta(\vec{r}) + \frac{1}{\rho} \frac{\partial}{\partial \theta} \nabla \cdot \vec{\Pi}(\vec{r}). \tag{17}$$

First, using eqs. (13), (14), and (15) from section 3.3.1, the divergence of $\vec{\Pi}(\vec{r})$, given in cylindrical coordinates as

$$\nabla \cdot \vec{\Pi}(\vec{r}) = \frac{1}{\rho} \frac{\partial}{\partial \rho}(\rho \Pi_\rho) + \frac{1}{\rho} \frac{\partial}{\partial \theta} \Pi_\theta + \frac{\partial}{\partial y} \Pi_y$$

may be straightforwardly obtained as follows:

$$\frac{1}{\rho} \frac{\partial}{\partial \rho}(\rho \Pi_\rho) = \frac{1}{j\omega\varepsilon_c} \sum_{n=-\infty}^{\infty} e^{jn\theta} \int_0^a \rho' \left[A_{\rho n}(\rho') \frac{1}{\rho} \frac{\partial}{\partial \rho}(\rho g_n^c) + A_{\theta n}(\rho') \frac{1}{\rho} \frac{\partial}{\partial \rho}(\rho g_n^s) \right] d\rho'$$

$$\frac{1}{\rho} \frac{\partial}{\partial \theta} \Pi_\theta = \frac{1}{j\omega\varepsilon_c} \sum_{n=-\infty}^{\infty} e^{jn\theta} \int_0^a \rho' \left[-A_{\rho n}(\rho') \frac{jn}{\rho} g_n^s + A_{\theta n}(\rho') \frac{jn}{\rho} g_n^c \right] d\rho'$$

$$\frac{\partial}{\partial y} \Pi_y = \frac{1}{j\omega\varepsilon_c} \sum_{n=-\infty}^{\infty} e^{jn\theta} \int_0^a \rho' \left[-A_{\rho n}(\rho') \frac{\partial^2}{\partial \rho' \partial y} g_n^e + A_{\theta n}(\rho') \frac{jn}{\rho'} \frac{\partial}{\partial y} g_n^e \right] d\rho'$$

and combining and collecting terms yields

$$\nabla\cdot\vec{\Pi} = \frac{1}{j\omega\varepsilon_c}\sum_{n=-\infty}^{\infty} e^{jn\theta}\int_0^a \rho'\Bigg\{A_{\rho n}(\rho')\left[\frac{1}{\rho}\frac{\partial}{\partial\rho}(\rho g_n^c) - \frac{jn}{\rho}\,g_n^s - \frac{\partial^2}{\partial\rho'\partial y}\,g_n^e\right]$$

$$+ A_{\theta n}(\rho')\left[\frac{1}{\rho}\frac{\partial}{\partial\rho}(\rho g_n^s) + \frac{jn}{\rho}\,g_n^c + \frac{jn}{\rho'}\frac{\partial}{\partial y}\,g_n^e\right]\Bigg\}\,d\rho'. \quad (18)$$

Utilizing relations (13), (14), and (18), the expressions for $E_\rho^s(\vec{r})$ and $E_\theta^s(\vec{r})$ given by eqs. (16) and (17), respectively, may be written as

$$E_\rho^s(\vec{r}) = -j\,\frac{\eta_c}{k_c}\sum_{n=-\infty}^{\infty} e^{jn\theta}\int_0^a \rho'\Bigg\{A_{\rho n}(\rho')\left[k_c^2\,g_n^c + \frac{\partial}{\partial\rho}\left(\frac{1}{\rho}\frac{\partial}{\partial\rho}(\rho g_n^c)\right) - \frac{\partial}{\partial\rho}\left(\frac{jn}{\rho}\,g_n^s\right)\right.$$

$$\left. - \frac{\partial^3}{\partial\rho\partial\rho'\partial y}\,g_n^e\right] + A_{\theta n}(\rho')\left[k_c^2\,g_n^s + \frac{\partial}{\partial\rho}\left(\frac{1}{\rho}\frac{\partial}{\partial\rho}(\rho g_n^s)\right)\right.$$

$$\left. + \frac{\partial}{\partial\rho}\left(\frac{jn}{\rho}\,g_n^c\right) + \frac{jn}{\rho'}\frac{\partial^2}{\partial\rho\partial y}\,g_n^e\right]\Bigg\}\,d\rho'$$

$$E_\theta^s(\vec{r}) = -j\,\frac{\eta_c}{k_c}\sum_{n=-\infty}^{\infty} e^{jn\theta}\int_0^a \rho'\Bigg\{A_{\rho n}(\rho')\left[-k_c^2 g_n^s + \frac{jn}{\rho^2}\frac{\partial}{\partial\rho}(\rho g_n^c) + \frac{n^2}{\rho^2}\,g_n^s\right.$$

$$\left. - \frac{jn}{\rho}\frac{\partial^2}{\partial\rho'\partial y}\,g_n^e\right] + A_{\theta n}(\rho')\left[k_c^2\,g_n^c + \frac{jn}{\rho^2}\frac{\partial}{\partial\rho}(\rho g_n^s)\right.$$

$$\left. - \frac{n^2}{\rho^2}\,g_n^c - \frac{n^2}{\rho\rho'}\frac{\partial}{\partial y}\,g_n^e\right]\,d\rho'$$

A more convenient form for the above equations involving E_ρ^s and E_θ^s may be expressed as

$$E_\rho^s(\vec{r}) = -j\,\frac{\eta_c}{k_c}\sum_{n=-\infty}^{\infty} e^{jn\theta}\int_0^a \left[A_{\rho n}(\rho')K_{\rho\rho}(\rho,\rho') + A_{\theta n}(\rho')K_{\rho\theta}(\rho,\rho')\right]\,d\rho' \quad (19)$$

$$E_\theta^s(\vec{r}) = -j\frac{\eta_c}{k_c}\sum_{n=-\infty}^{\infty} e^{jn\theta}\int_0^a\left[A_{\rho n}(\rho')K_{\theta\rho}(\rho,\rho') + A_{\theta n}(\rho')K_{\theta\theta}(\rho,\rho')\right]d\rho' \quad (20)$$

where the $K_{\alpha\beta}$'s are defined as

$$K_{\rho\rho}(\rho,\rho',y) = \rho'\left[k_c^2\, g_n^c + \frac{\partial}{\partial\rho}\left(\frac{1}{\rho}\frac{\partial}{\partial\rho}(\rho g_n^c)\right) - \frac{\partial}{\partial\rho}\left(\frac{jn}{\rho}\, g_n^s\right) - \frac{\partial^3}{\partial\rho\partial\rho'\partial y}\, g_n^e\right] \quad (21a)$$

$$K_{\rho\theta}(\rho,\rho',y) = \rho'\left[k_c^2\, g_n^s + \frac{\partial}{\partial\rho}\left(\frac{1}{\rho}\frac{\partial}{\partial\rho}(\rho g_n^s)\right) + \frac{\partial}{\partial\rho}\left(\frac{jn}{\rho}\, g_n^c\right) + \frac{jn}{\rho'}\frac{\partial^2}{\partial\rho\partial y}\, g_n^e\right] \quad (21b)$$

$$K_{\theta\rho}(\rho,\rho',y) = \rho'\left[-k_c^2 g_n^s + \frac{jn}{\rho^2}\frac{\partial}{\partial\rho}(\rho g_n^c) + \frac{n^2}{\rho^2}\, g_n^s - \frac{jn}{\rho}\frac{\partial^2}{\partial\rho'\partial y}\, g_n^e\right] \quad (21c)$$

$$K_{\theta\theta}(\rho,\rho',y) = \rho'\left[k_c^2\, g_n^c + \frac{jn}{\rho^2}\frac{\partial}{\partial\rho}(\rho g_n^s) - \frac{n^2}{\rho^2}\, g_n^c - \frac{n^2}{\rho\rho'}\frac{\partial}{\partial y}\, g_n^e\right]. \quad (21d)$$

By using the previous components of electric field expressed in eqs. (19) and (20), the polar component IE's describing the circular patch can be obtained. Since the patch is perfectly conducting, the total electric field tangential to the patch surface (y=0) must vanish, which may be stated as $E_\rho^s(\vec{r}) = -E_\rho^i(\vec{r})|_{y=0}$ and $E_\theta^s(\vec{r}) = -E_\theta^i(\vec{r})|_{y=0}$ where $E_{\rho,\theta}^i(\vec{r})$ is the incident field exciting the patch. With the help of expressions (19) and (20) these boundary conditions lead to

$$\sum_{n=-\infty}^{\infty} e^{jn\theta}\int_0^a\left[A_{\rho n}(\rho')K_{\rho\rho}(\rho,\rho') + A_{\theta n}(\rho')K_{\rho\theta}(\rho,\rho')\right]\Big|_{y=0}d\rho' = -j\frac{k_c}{\eta_c}E_\rho^i(\rho,\theta,y=0)$$

$$\sum_{n=-\infty}^{\infty} e^{jn\theta}\int_0^a\left[A_{\rho n}(\rho')K_{\theta\rho}(\rho,\rho') + A_{\theta n}(\rho')K_{\theta\theta}(\rho,\rho')\right]\Big|_{y=0}d\rho' = -j\frac{k_c}{\eta_c}E_\theta^i(\rho,\theta,y=0).$$

(It must be remembered that the $K_{\alpha\beta}$'s have derivatives with respect to y present. These derivatives must be calculated before y=0 can be evalated in the previous two EFIE's.) By invoking the results previously illustrated in section 2.3, the above two equations lead to the following IE's for the resonant patch currents:

$$\sum_{n=-\infty}^{\infty} e^{jn\theta} \int_0^a \left[A_{\rho n}(\rho') K_{\rho\rho}(\rho,\rho') + A_{\theta n}(\rho') K_{\rho\theta}(\rho,\rho') \right] d\rho' = 0 \quad \vec{\rho} \in s \tag{22}$$

$$\sum_{n=-\infty}^{\infty} e^{jn\theta} \int_0^a \left[A_{\rho n}(\rho') K_{\theta\rho}(\rho,\rho') + A_{\theta n}(\rho') K_{\theta\theta}(\rho,\rho') \right] d\rho' = 0 \quad \vec{\rho} \in s. \tag{23}$$

Although expressions (22) and (23) are in a rather cumbersome series form, exploting the orthogonality of the exponential permits them to be simplified as

$$\int_0^a \left[A_{\rho n}(\rho') K_{\rho\rho}(\rho,\rho') + A_{\theta n}(\rho') K_{\rho\theta}(\rho,\rho') \right] d\rho' = 0 \qquad \begin{matrix} n = 0, \pm 1, \pm 2, \ldots \\ \vec{\rho} \in s \end{matrix} \tag{24}$$

$$\int_0^a \left[A_{\rho n}(\rho') K_{\theta\rho}(\rho,\rho') + A_{\theta n}(\rho') K_{\theta\theta}(\rho,\rho') \right] d\rho' = 0 \qquad \begin{matrix} n = 0, \pm 1, \pm 2, \ldots \\ \vec{\rho} \in s \end{matrix} \tag{25}$$

which are now coupled IE's that can be solved independently for each n. For the special case of n=0, the above equations decouple forming two IE's which can be solved independently. Physically, when eqs. (24) and (25) decouple, they describe resonant modes on the patch in which currents sustained at resonance are axially symmetric. The solution of these axially symmetric modes is furnished in the subsequent chapter.

3.4 SUMMARY

The Green's function presented in Chapter II can be alternatively represented in polar form as

$$\left[G_{\alpha\beta}(\vec{r}|\vec{r}')\right] = \begin{bmatrix} G_t\cos(\theta-\theta') & G_t\sin(\theta-\theta') & 0 \\ -G_t\sin(\theta-\theta') & G_t\cos(\theta-\theta') & 0 \\ -\frac{\partial}{\partial\rho'}G_c & -\frac{1}{\rho'}\frac{\partial}{\partial\theta'}G_c & G_n \end{bmatrix} \tag{26}$$

with

$$G_{t,n} = \int_0^\infty J_o(\lambda|\vec{\rho}-\vec{\rho}'|)\,\frac{e^{-p_c|y-y'|} + R_{t,n}(\lambda)\,e^{-p_c(y+y')}}{4\pi p_c}\,\lambda d\lambda$$

$$G_c = \int_0^\infty J_o(\lambda|\vec{\rho}-\vec{\rho}'|)\,\frac{C(\lambda)\,e^{-p_c(y+y')}}{4\pi p_c}\,\lambda d\lambda.$$

This polar representation allows $\overleftrightarrow{G}$ to be conveniently applied to a circular patch embedded in the tri-layered medium.

The Hertzian potential maintained in the cover by the radiating patch can be suitably expressed by implementing relation (26) and expanding $\vec{K}(\vec{r}')$ in an angular Fourier series. Once this is done, $\vec{\Pi}(\vec{r})$ can be analytically integrated with respect to θ leading to a relatively simplified form. By utilizing this convenient expression for the Hertz potential (eqs. (3.13), (3.14), (3.15)), the necessary components of electric field, E_ρ^s and E_θ^s, scattered from the surface the patch can be constructed (eqs. (3.19) and (3.20)). Once these components of electric

field are determined, the boundary condition on the perfectly conducting patch surface (y=0) leads to IE's for the resonant patch currents:

$$\sum_{n=-\infty}^{\infty} e^{jn\theta} \int_0^a \left[A_{\rho n}(\rho') K_{\rho\rho}(\rho,\rho') + A_{\theta n}(\rho') K_{\rho\theta}(\rho,\rho') \right] d\rho' = 0 \quad \vec{\rho} \in s \tag{3.22}$$

$$\sum_{n=-\infty}^{\infty} e^{jn\theta} \int_0^a \left[A_{\rho n}(\rho') K_{\theta\rho}(\rho,\rho') + A_{\theta n}(\rho') K_{\theta\theta}(\rho,\rho') \right] d\rho' = 0 \quad \vec{\rho} \in s. \tag{3.23}$$

Exploiting the orthogonality of $e^{jn\theta}$ simplifies the above system to

$$\int_0^a \left[A_{\rho n}(\rho') K_{\rho\rho}(\rho,\rho') + A_{\theta n}(\rho') K_{\rho\theta}(\rho,\rho') \right] d\rho' = 0 \qquad \begin{matrix} n = 0, \pm 1, \pm 2, \ldots \\ \vec{\rho} \in s \end{matrix} \tag{3.24}$$

$$\int_0^a \left[A_{\rho n}(\rho') K_{\theta\rho}(\rho,\rho') + A_{\theta n}(\rho') K_{\theta\theta}(\rho,\rho') \right] d\rho' = 0 \qquad \begin{matrix} n = 0, \pm 1, \pm 2, \ldots \\ \vec{\rho} \in s \end{matrix} \tag{3.25}$$

which are now coupled IE's that may be solved independently for each n (n representing the various modes of resonances on the patch).

CHAPTER IV

SOLUTION TO DECOUPLED AXIALLY-SYMMETRIC RESONANT IE'S

4.1 INTRODUCTION

Pursuing a moment-method solution of the coupled IE's, eqs. (3.24) and (3.25), via Galerkin's method, enables the exact determination of complex resonant frequencies (which include radiation damping) and corresponding resonant currents for the circular patch. The special case of n=0 causes a decoupling of the IE's, subsequently providing two independent IE's which describe angularly invariant eigenmodes on the patch. The solution of these independent IE's is pursued in this chapter.

Section 4.2 presents the details involved in decoupling the IE's. When n equals zero the coupling kernels, $K_{\rho\theta}$ and $K_{\theta\rho}$, implicated in eqs. (3.24) and (3.25) vanish, while the self terms, $K_{\rho\rho}$ and $K_{\theta\theta}$, simplify immensely. The expressions for $K_{\rho\rho}$ and $K_{\theta\theta}$ may then be expanded leading to relatively simple forms of the independent IE's.

Once the IE's are placed in an appropriate form, Galerkin's method may be applied. Tchebychev polynomials, with the expected edge singularities incorporated, provide a suitable choice of basis and testing functions which may be utilized in both IE's. Once expansion and testing are carried out, an N×N homogeneous matrix equation results from each IE. The only nontrivial solution to these matrix equations requires a vanishing determinant. This condition leads to the

determination of the desired complex resonant frequencies for the circular patch.

In section 4.4, the search for the previously mentioned complex frequencies is pursued. The evaluation of each element involved when calculating the determinant described above requires numeric evaluation of a spectral inversion integral in which many subtleties are present. The spectral integrals all share common branch point and pole singularities. The proper choice of the branch cut and the location of the poles strongly influence the correct choice of integration path that must be used. Once the spectral integrals are correctly evaluated the complex resonant frequencies and corresponding patch currents are obtained. Numerical results for the resonant mode in which only a radial component of current exist are presented.

4.2 AXIALLY SYMMETRIC DECOUPLING FOR n=0

In order to illustrate the decoupling of (3.24) and (3.25), the expressions for g_n^e, g_n^c, and g_n^s , eqs. (3.11) and (3.12), must be specialized for n=0. This task involves first, calculating f_n^e, f_n^c, and f_n^s when n=0. From expression (3.9) it easily seen that

$$f_o^e = 2\pi J_o(\lambda\rho)J_o(\lambda\rho'). \tag{1}$$

Also, expression (3.10) specializes to

$$f_o^{\substack{c\\s}} = \begin{Bmatrix} 1 \\ -j \end{Bmatrix} \pi\left[J_{-1}(\lambda\rho)J_{-1}(\lambda\rho') \pm J_1(\lambda\rho)J_1(\lambda\rho')\right]$$

which, with the help of the relation

$$J_{-n}(z) = (-1)^n J_n(z) \qquad ([10],\ p.358) \tag{2}$$

simplifies further to

$$f_o^c = 2\pi J_1(\lambda\rho)J_1(\lambda\rho') \tag{3}$$

$$f_o^s = 0. \tag{4}$$

Thus, utilizing eqs. (1), (3), and (4), g_o^e, g_o^c, and g_o^s simply become

$$g_o^e = \int_0^\infty \frac{\lambda C(\lambda)}{2p_c}\, e^{-p_c y} J_o(\lambda\rho)J_o(\lambda\rho')\, d\lambda \tag{5}$$

$$g_o^c = \int_0^\infty \lambda\, \frac{1 + R_t(\lambda)}{2p_c}\, J_1(\lambda\rho)J_1(\lambda\rho')\, d\lambda \tag{6}$$

$$g_o^s = 0 \tag{7}$$

where the fact that $y=y'=0$ has been exercised everywhere except for g_o^e. This reason for this, as it will soon be seen, is that $\frac{\partial}{\partial y} g_o^e$ must first be evaluated.

With g_o^e and g_s^c conveniently expressed, the $K_{\alpha\beta}$'s --represented in eqs. (3.21a)-(3.21d)-- may be readily evaluated showing the decoupling and simplification of the IE's for the mode n=0. Concentrating first on decoupling the equations, it is easily observed that the expressions for $K_{\rho\theta}$ and $K_{\theta\rho}$,

$$K_{\rho\theta}(\rho,\rho') = \rho'\left[k_c^2\, g_n^s + \frac{\partial}{\partial\rho}\left(\frac{1}{\rho}\frac{\partial}{\partial\rho}(\rho g_n^s)\right) + \frac{\partial}{\partial\rho}\left(\frac{jn}{\rho}\, g_n^c\right) + \frac{jn}{\rho'}\frac{\partial^2}{\partial\rho\partial y}\, g_n^e\right] \tag{3.21b}$$

$$K_{\theta\rho}(\rho,\rho') = \rho'\left[-k_c^2 g_n^s + \frac{jn}{\rho^2}\frac{\partial}{\partial\rho}(\rho g_n^c) + \frac{n^2}{\rho^2} g_n^s - \frac{jn}{\rho}\frac{\partial^2}{\partial\rho'\partial y} g_n^e\right] \qquad (3.22c)$$

vanish when n=0 since all terms depend either on n or g_o^s. Thus, IE's (3.24) and (3.25) decouple becoming the independent IE's

$$\int_0^a A_\rho(\rho')\, K_{\rho\rho}(\rho,\rho')\, d\rho' = 0$$

$$\int_0^a A_\theta(\rho')\, K_{\theta\theta}(\rho,\rho')\, d\rho' = 0.$$

Further, by again applying relations (5), (6), and (7), $K_{\rho\rho}$ and $K_{\theta\theta}$ -- expressions (3.21a) and (3.21d)-- become

$$K_{\rho\rho}^o = \rho'\left[k_c^2 g_o^c + \frac{\partial}{\partial\rho}\left(\frac{1}{\rho}\frac{\partial}{\partial\rho}(\rho g_o^c)\right) - \frac{\partial^3}{\partial\rho\partial\rho'\partial y} g_o^e\right]$$

$$= \rho'\left[(k_c^2 - \frac{1}{\rho^2})g_o^c + \frac{1}{\rho}\frac{\partial}{\partial\rho} g_o^c + \frac{\partial^2}{\partial\rho^2} g_o^c - \frac{\partial^3}{\partial\rho\partial\rho'\partial y} g_o^e\right] \qquad (8)$$

$$K_{\theta\theta}^o = \rho'\left[k_c^2 g_o^c\right]$$

where the superscript o denotes n=0.

$K_{\theta\theta}^o$ is already in a suitable form. On the other hand, $K_{\rho\rho}^o$ must be modified further. With the assistance of relation relation (5), the first three terms in eq. (8) may be combined as

$$\int_0^\infty \lambda \frac{1 + R_t(\lambda)}{2p_c} J_1(\lambda\rho')\left[(k_c^2 - \frac{1}{\rho^2}) + \frac{1}{\rho}\frac{\partial}{\partial\rho} + \frac{\partial^2}{\partial\rho^2}\right] J_1(\lambda\rho)\, d\lambda.$$

Adding and subtracting the quantity $\lambda^2 J_1(\lambda\rho)$ leads to

$$\int_0^\infty \lambda \frac{1 + R_t(\lambda)}{2p_c} J_1(\lambda\rho')\left[\frac{\partial^2}{\partial\rho^2} + \frac{1}{\rho}\frac{\partial}{\partial\rho} + (\lambda^2 - \frac{1}{\rho^2})\right]J_1(\lambda\rho)\, d\lambda$$

$$+ \int_0^\infty \lambda \frac{1 + R_t(\lambda)}{2p_c} J_1(\lambda\rho')\left[k_c^2 - \lambda^2\right]J_1(\lambda\rho)\, d\lambda. \qquad (9)$$

By virtue of Bessel's differential equation

$$\frac{\partial^2}{\partial r^2} R + \frac{1}{r}\frac{\partial}{\partial r} R + (T - \frac{\nu^2}{r^2}) R = 0 \qquad ([11], p.364)$$

with solutions defined as Bessel functions of the first kind with order ν and argument Tr ($R=J_\nu(Tr)$), the first term in expression (9) vanishes ($\nu=1$, $T=\lambda$). Thus, $K^o_{\rho\rho}$ becomes

$$K^o_{\rho\rho} = \rho'\left[\int_0^\infty \lambda \frac{1 + R_t(\lambda)}{2p_c}\left[k_c^2 - \lambda^2\right]J_1(\lambda\rho)J_1(\lambda\rho')\, d\lambda - \frac{\partial^3}{\partial\rho\partial\rho'\partial y} g^e_o\right] \qquad (10)$$

but this is not yet the desired form; the derivatives on g^e_o still have to be evaluated in the last term. Continuing on, with the use of relation (5), this term can be expressed as

$$\frac{\partial^3}{\partial\rho\partial\rho'\partial y} g^e_o = \int_0^\infty \frac{\lambda C(\lambda)}{2p_c}\frac{\partial}{\partial y} e^{-p_c y} \frac{\partial^2}{\partial\rho\partial\rho'}\left(J_o(\lambda\rho)J_o(\lambda\rho')\right) d\lambda. \qquad (11)$$

Carrying out the derivatives and evaluating at the patch surface (y=0) leads to

$$\frac{\partial^3}{\partial\rho\partial\rho'\partial y}\, g_o^e = -\int_0^\infty \frac{\lambda^3 C(\lambda)}{2}\, J_1(\lambda\rho)J_1(\lambda\rho')\, d\lambda \tag{12}$$

where the chain rule, $\frac{\partial}{\partial x}\, J_1(\alpha x) = \alpha J_1'(\alpha x)$, and the relation $J_o'(z) = -J_1(z)$ ([10], p.361) were applied in passing from eq. (11) to eq. (12). Thus, substituting relation (12) back into eq. (10) yields

$$K^o_{\rho\rho} = \rho'\int_0^\infty \left[\lambda\, \frac{1 + R_t(\lambda)}{2p_c}\, (k_c^2 - \lambda^2) + \frac{\lambda^3 C(\lambda)}{2}\right] J_1(\lambda\rho)J_1(\lambda\rho')\, d\lambda$$

which is the desired form for $K^o_{\rho\rho}$.

To briefly summarize, for n=0 the IE's represented in eqs. (3.24) and (3.25) decouple and simplify immensely leading to independent IE's expressed as

$$\int_0^a A_\rho(\rho')\, K_{\rho\rho}(\rho,\rho')\, d\rho' = 0 \tag{13}$$

$$\int_0^a A_\theta(\rho')\, K_{\theta\theta}(\rho,\rho')\, d\rho' = 0 \tag{14}$$

where

$$K^o_{\theta\theta} = \rho' k_c^2 \int_0^\infty \lambda\, \frac{1 + R_t(\lambda)}{2p_c}\, J_1(\lambda\rho)J_1(\lambda\rho')\, d\lambda \tag{15}$$

$$K^o_{\rho\rho} = \rho'\int_0^\infty \left[\lambda\, \frac{1 + R_t(\lambda)}{2p_c}\, (k_c^2 - \lambda^2) + \frac{\lambda^3 C(\lambda)}{2}\right] J_1(\lambda\rho)J_1(\lambda\rho')\, d\lambda \tag{16}$$

$$K^{o}_{\rho\theta} = K^{o}_{\theta\rho} = 0.$$

With a judicious choice of basis functions representing the radially-dependent current amplitudes $A_{\rho}(\rho')$ and $A_{\theta}(\rho')$, Galerkin's method can be successfully applied to (13) and (14). This will ultimately lead to numerical solutions providing both resonant frequencies and current distributions, as will be shown in the following sections.

4.3 MoM SOLUTION VIA GALERKIN'S METHOD

The IE's as expressed in eqs. (13) and (14) describe unique resonant modes on the circular patch. EFIE (13) describes modes where the surface current sustained at resonance has only a radial component with no azimuthal variation. EFIE (14), on the other hand, describes modes where the surface current sustained at resonance has only a circumferential component but is also azimuthally invariant. Applying a moment-method solution, namely, Galerkin's method, to IE's (13) and (14) will produce a system of equations from which the complex resonant frequencies and corresponding current distributions for these simple modes can be obtained.

Galerkin's method, as applied in this situation, involves expanding the unknown current distributions (represented by amplitudes $A_{\rho}(\rho')$ and $A_{\theta}(\rho')$ in IE's (13) and (14)) in a set of N basis functions which are complete, physically realizable, and enable the spatial integration evident in the IE's to be evaluated in closed form. Once expansion is completed, the resulting equations are integrated again over the entire domain of the patch into the identical set of N functions used for ex-

pansion. This last procedure, better known as testing, results in a N×N linear system of equations for each mode, which in turn can be solved to yield the desired resonant frequencies and current distributions. The number of basis functions (and therefore testing functions) to be used depends on the desired accuracy of the resultant resonant frequency and current distributions. Theoretically, to yield exact results N should extend to infinity. Numerically this is impossible and for all practical purposes the number of basis functions needed for satisfactory convergence is fairly low.

4.3.1 RADIAL MODE

Seeking a complete set of basis functions for $A_\rho(\rho')$, which when multiplied by $\rho' J_1(\lambda\rho')$ can be analytically integrated from $\rho'=0$ to $\rho'=a$, leads to the consideration of the Tchebychev polynomials $T_m(\rho'/a)$ ([10], p. 778). Although with some minor manipulations these functions are integrable with $\rho' J_1(\lambda\rho')$, they must be modified to accommodate the physical behavior of the expected patch current distribution. By naively representing $A_\rho(\rho')$ as

$$A_\rho(\rho') = \sum_{m=0}^{\infty} A_{\rho m} T_m(\rho'/a) \tag{17}$$

it is evident that the known edge condition of vanishing normal current at an infinitely thin edge (in this case the edge being $\rho=a$) is not present; therefore, expression (17) must be modified to

$$A_\rho(\rho')=\sum_{m=0}^{\infty} A_{\rho m} T_m(\rho'/a)\sqrt{1-(\rho'/a)^2}\,. \tag{18}$$

Further, by virtue of the polar coordinate representation $\vec{K} = \hat{\rho}K_\rho$, there is the possibility of a discontinuity in the current or it's derivatives at ρ=0. But it has been shown by Blischke [12] that this problem may be circumvented by retaining only the odd terms in expression (18) (Blischke has rigorously demonstrated that the even terms in relation (18) identically equal zero). Thus, $A_\rho(\rho')$ ultimately becomes

$$A_\rho(\rho') = \sum_{m=0}^{\infty} A_{\rho m} T_{2m+1}(\rho'/a)\sqrt{1-(\rho'/a)^2}\,. \tag{19}$$

With $A_\rho(\rho')$ represented in this form, the spatial integration involved in IE (13) can conveniently be handled. By utilizing relation (19) and exploiting the linearity of the summation and integration operators, IE (13) may be written as

$$\sum_{m=0}^{\infty} A_{\rho m} \int_0^a T_{2m+1}(\rho'/a)\sqrt{1-(\rho'/a)^2}\; K^o_{\rho\rho}(\rho,\rho')\, d\rho' = 0. \tag{20}$$

Considering only the spatial integration and the relevant terms in eq. (20) leads to the required evaluation of

$$I_{m1} = \int_0^a T_{2m+1}(\rho'/a)\sqrt{1-(\rho'/a)^2}\; J_1(\lambda\rho')\, \rho' d\rho'$$

Using the substitution $u=\rho'/a$ and rewriting the square root term leads

to

$$I_{m1} = a^2 \int_0^1 T_{2m+1}(u) \frac{u(1 - u^2)}{\sqrt{1 - u^2}} J_1(\lambda a u)\, du. \qquad (21)$$

By repeated application of the recursion relation

$$2uT_n(u) = T_{n-1}(u) + T_{n+1}(u) \qquad ([13]\ p.1032)$$

the quantity $u(1 - u^2)T_{2m+1}(u)$ evident in eq. (21) can be expressed as

$$\frac{1}{8}\left[T_{2m}(u) + T_{2m+2}(u) + T_{|2m-2|}(u) + T_{2m+4}(u)\right]. \qquad (22)$$

(The details omitted in obtaining eq. (22) and an explanation of the absolute value apparent in the third term are provided in Appendix B.) Utilizing expression (22) allows eq. (21) to become

$$I_{m1} = \frac{a}{8}^2 \int_0^1 \left[T_{2m}(u) + T_{2m+2}(u) + T_{|2m-2|}(u) + T_{2m+4}(u)\right] \frac{J_1(\lambda a u)}{\sqrt{1 - u^2}}\, du. \qquad (23)$$

With the help of

$$\int_0^1 \frac{T_n(x)\, J_\nu(yx)}{\sqrt{1 - x^2}}\, dx = \frac{\pi}{2} J_{\frac{\nu+n}{2}}\left(\frac{y}{2}\right) J_{\frac{\nu-n}{2}}\left(\frac{y}{2}\right) \qquad \begin{array}{l} y > 0 \\ \mathrm{Re}(\nu) > -n-1 \end{array}$$

[13], the spatial integration is finally evaluated as

$$I_{m1} = \frac{\pi a^2}{16}\left[J_{\frac{1+2m}{2}}(\frac{\lambda a}{2})\ J_{\frac{1-2m}{2}}(\frac{\lambda a}{2}) + J_{\frac{2m+3}{2}}(\frac{\lambda a}{2})\ J_{\frac{-2m-1}{2}}(\frac{\lambda a}{2})\right.$$

$$\left. - J_{\frac{1+|2m-2|}{2}}(\frac{\lambda a}{2})\ J_{\frac{1-|2m-2|}{2}}(\frac{\lambda a}{2}) + J_{\frac{2m+5}{2}}(\frac{\lambda a}{2})\ J_{\frac{-2m-3}{2}}(\frac{\lambda a}{2})\right]$$

$$= \frac{\pi a^2}{16}\ \tilde{J}_m(\lambda a). \qquad (24)$$

Using this result, EFIE (20) may be expressed as

$$\frac{\pi a^2}{16}\sum_{m=0}^{N} A_{\rho m}\int_0^{\infty}\left[\lambda\ \frac{1 + R_t(\lambda)}{2p_c}\ (k_c^2 - \lambda^2) + \frac{\lambda^3 C(\lambda)}{2}\right] J_1(\lambda\rho)\tilde{J}_m(\lambda a)\ d\lambda = 0. \qquad (25)$$

Now that current expansion has been completed, testing can be implemented. By multiplying the above with

$$T_{2l+1}(\rho'/a)\ \sqrt{1 - (\rho'/a)^2}$$

and integrating over the surface of the patch, the following spatial integral results:

$$I_{l1} = \int_s T_{2l+1}(\rho/a)\sqrt{1 - (\rho/a)^2}\ J_1(\lambda\rho)\ ds$$

$$= 2\pi\int_0^a T_{2l+1}(\rho/a)\sqrt{1 - (\rho/a)^2}\ J_1(\lambda\rho)\rho\ d\rho.$$

Application of result (24) allows the above integral to be evaluated as

$$I_{l1} = \frac{\pi^2 a^2}{8}\left[J_{\frac{1+2l}{2}}(\frac{\lambda a}{2})\ J_{\frac{1-2l}{2}}(\frac{\lambda a}{2}) + J_{\frac{2l+3}{2}}(\frac{\lambda a}{2})\ J_{\frac{-2l-1}{2}}(\frac{\lambda a}{2})\right.$$

$$\left. - J_{\frac{1+|2l-2|}{2}}(\frac{\lambda a}{2})\ J_{\frac{1-|2l-2|}{2}}(\frac{\lambda a}{2}) + J_{\frac{2l+5}{2}}(\frac{\lambda a}{2})\ J_{\frac{-2l-3}{2}}(\frac{\lambda a}{2})\right]$$

$$= \frac{\pi^2 a^2}{8}\tilde{J}_l(\lambda a). \tag{26}$$

Thus, EFIE (25) becomes the matrix equation

$$\sum_{m=0}^{N} A_{\rho m} B_{lm} = 0 \qquad l = 0,1,2,\ldots,N \tag{27}$$

where

$$B_{lm} = \int_0^{\infty}\left[\lambda\ \frac{1 + R_t(\lambda)}{2p_c}\ (k_c^2 - \lambda^2) + \frac{\lambda^3 C(\lambda)}{2}\right]\tilde{J}_m(\lambda a)\tilde{J}_l(\lambda a)\ d\lambda. \tag{28}$$

The difficulty of solving IE (13) has been reduced to solving a linear system of equations evident in eq. (27). Non-trivial solutions to this system impose the condition of a vanishing determinant. This condition, DET[B(ω)]=0, enables the numerical extraction of the complex resonant frequencies. Complications arise though, due to the necessary evaluation of the spectral integrals obvious in the matrix elements B_{lm}.

4.3.2 CIRCUMFERENTIAL MODE

The tedious details involved in applying Galerkin's method to EFIE (14) are similar to those implemented in the MoM solution of IE (13). The same set of basis functions used for $A_\rho(\rho')$ may be used to expand

$A_\theta(\rho')$, but the correct edge condition must be incorporated. For the circumferential mode, the current (which is tangential to the patch edge) must become appropriately singular at the edge (ρ=a) which leads to

$$A_\theta(\rho') = \sum_{m=0}^{\infty} A_{\theta m} \frac{T_{2m+1}(\rho'/a)}{\sqrt{1 - (\rho'/a)^2}}. \tag{29}$$

(Again only the odd terms are considered to assure continuity of the polar coordinate representation $\vec{K} = K_\theta \hat{\theta}$ [12].) Substituting expansion (29) into IE (14) yields

$$\sum_{m=0}^{N} A_{\theta m} \int_0^a \frac{T_{2m+1}(\rho'/a)}{\sqrt{1 - (\rho'/a)^2}} K^o_{\theta\theta}(\rho,\rho')\, d\rho' = 0. \tag{30}$$

In analogy with section 4.3.1, the spatial integration in IE (30) may be evaluated creating

$$\sum_{m=0}^{N} A_{\theta m} k_c^2 \int_0^{\infty} \lambda \frac{1 + R_t(\lambda)}{2p_c} J_1(\lambda\rho) \hat{J}_m(\lambda a)\, d\lambda = 0. \tag{31}$$

Continuing on, and applying the testing operator

$$\int_s \frac{T_{2m+1}(\rho'/a)}{\sqrt{1 - (\rho'/a)^2}} (\text{ eq. } 31)\, ds$$

leads to the following homogeneous matrix equation for the circumferential mode current amplitudes:

$$\sum_{m=0}^{N} A_{\theta m} C_{lm} = 0 \qquad l = 0,1,2,\ldots,N \tag{32}$$

where

$$C_{lm} = \int_0^{\infty} \lambda \, \frac{1 + R_t(\lambda)}{2p_c} \, \hat{J}_l(\lambda a) \, \hat{J}_m(\lambda a) \, d\lambda \tag{33}$$

with

$$\hat{J}_p(\lambda a) = \left[J_{\frac{1+2p}{2}}(\tfrac{\lambda a}{2}) \; J_{\frac{1-2p}{2}}(\tfrac{\lambda a}{2}) + J_{\frac{2p+3}{2}}(\tfrac{\lambda a}{2}) \; J_{\frac{-2p-1}{2}}(\tfrac{\lambda a}{2}) \right] \quad \text{for } p=l,m.$$

As witnessed in last section, complex resonant frequencies may be extracted from (32) leading to the construction of $A_\theta(\rho')$. Again problems arise in the numerical evaluation of the inversion integral. The subtle difficulties, which are present in both spectral integrals (28) and (33), are addressed in detail in the subsequent section.

4.4 NUMERICAL EVALUATION

To illustrate the complications that arise when evaluating inversion integrals (28) and (33), it is convenient to utilize the expressions for $R_t(\lambda)$ and $C(\lambda)$ in section 2.2 to express B_{lm} and C_{lm} as

$$B_{lm} = \int_0^{\infty} \left[\frac{(k_c^2 - \lambda^2)\lambda}{Z^h(\lambda)} + \frac{\lambda^3 (N_{fc}^2 - 1) p_c}{Z^h(\lambda) Z^e(\lambda)} \right] \tilde{J}_l(\lambda a) \tilde{J}_m(\lambda a) \, d\lambda \tag{34}$$

$$C_{lm} = \int_0^{\infty} \frac{\lambda}{Z^h(\lambda)} \hat{J}_l(\lambda a)\hat{J}_m(\lambda a)\, d\lambda \qquad (35)$$

with $\quad Z^h(\lambda) = p_c + p_f \coth(p_f t) \qquad Z^e(\lambda) = N_{fc}^2 p_c + p_f \tanh(p_f t).$

The real line integration as implicated above must be implemented with due regard to the branch point and pole singularities present. To accommodate the evaluation of the above integrals it is necessary to invoke Cauchey's theorem for contour integrals [14]. This theorem along with proper determination of the implicated branch cuts, allows for the correct numerical evaluation of the above integrals.

4.4.1 COMPLEX PLANE SINGULARITIES

Analysis of integral representation (34) suffices to demonstrate the procedure which can be utilized to evaluate both spectral integrals (34) and (35).

The integrand in eq. (34) has a complicated functional dependence on the wavenumber parameter $p_c = \sqrt{\lambda - k_c}\,\sqrt{\lambda + k_c}$. It is evident that branch cuts emanating from branch points at $\lambda = \pm k_c$ are implicated by the square roots in order to render the integrand in eq. (34) analytic. (Branch cut singularities of p_f are not implicated since the integrand is an even function of this quantity.) Considering the media to be slightly lossy with $k_c = k_c' - jk_c''$ and $k_c'' > 0$ leads to the determination of the standard hyperbolic branch cuts [5]. These branch cuts along with the surface wave poles, apparent when $Z^h(\lambda)=0$ (TE_{odd} pole) and $Z^e(\lambda)=0$ (TM_{even} pole), are depicted in Figure 3. The branch cuts are chosen to

satisfy the physical constraints which require waves to decay and propagate outward from a source point. These conditions, which are consistent with the exponential factors of the form $e^{-p_c y}$ implicated throughout this analysis, require $Re\{p_c\}>0$ and $Im\{p_c\}>0$.

When considering the resonance of the circular patch, though, it is obvious that in order to have fields decay temporally due to radiation, the imaginary part of ω (and therefore k_c) must become positive in order to be consistent with the $e^{j\omega t}$ time dependence. This results in a "migration" of the branch cuts and poles [1] in Figure 3 across the real axis. When this "migration" occurs, the branch cuts to no longer separate the proper Riemann sheets which guarantee $Re\{p_c\}>0$ and the $Im\{p_c\}>0$; the natural resonant modes are consequently non-spectral leaky modes. Although this seems contradictory, similar branch cut analysis has been used by Chew and Kong [1,2,15] which has produced reasonable numerical results predicting characteristics of resonant structures. Thus, the accepted and apparently correct configuration of the complex-plane singularities implicated in the resonant circular patch analysis, is illustrated in Figure 4. It is noted that the imaginary parts of all the singularities are very small. These imaginary parts are exaggerated, and appear to be significant in the figures only for the purpose of illustration.

4.4.2 PATH OF INTEGRATION

Since the integration path implicated in expression (34) passes from zero to infinity, only the right hand side of the complex λ plane need be considered when determining the proper path of integration.

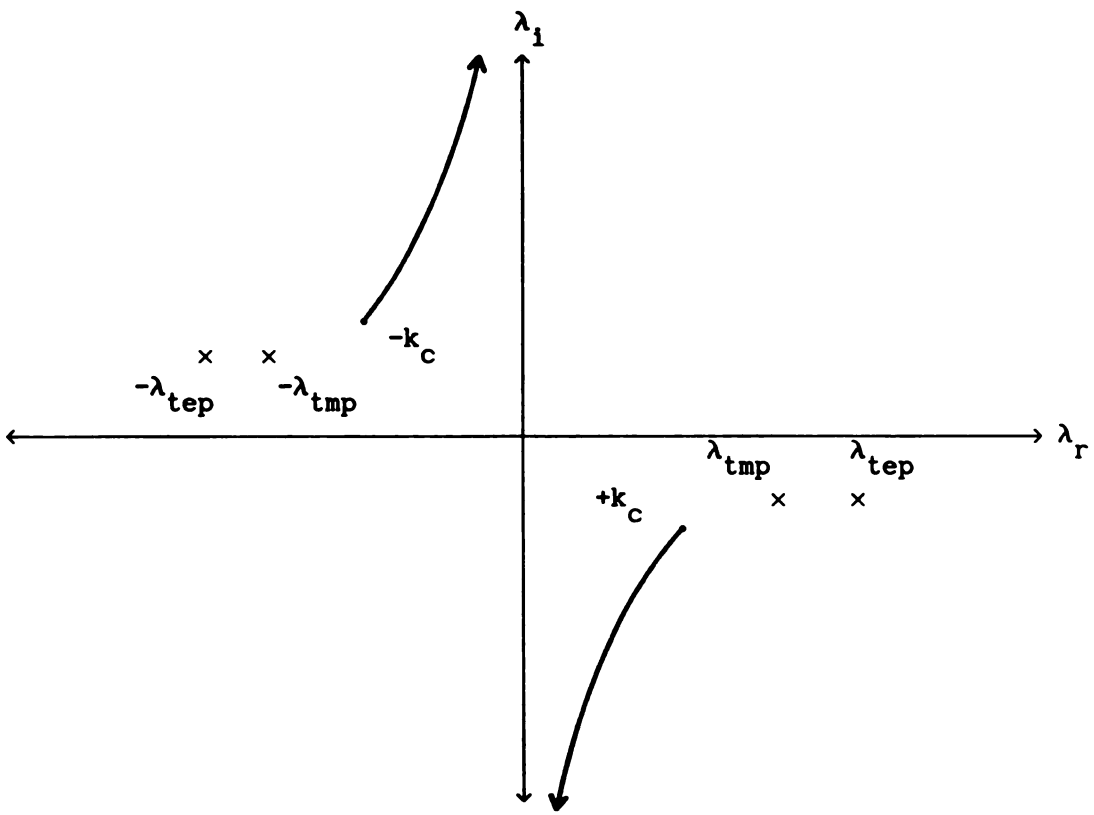

Figure 3. Standard hyperbolic branch cuts along with TE and TM surface wave pole singularities in the complex λ plane.

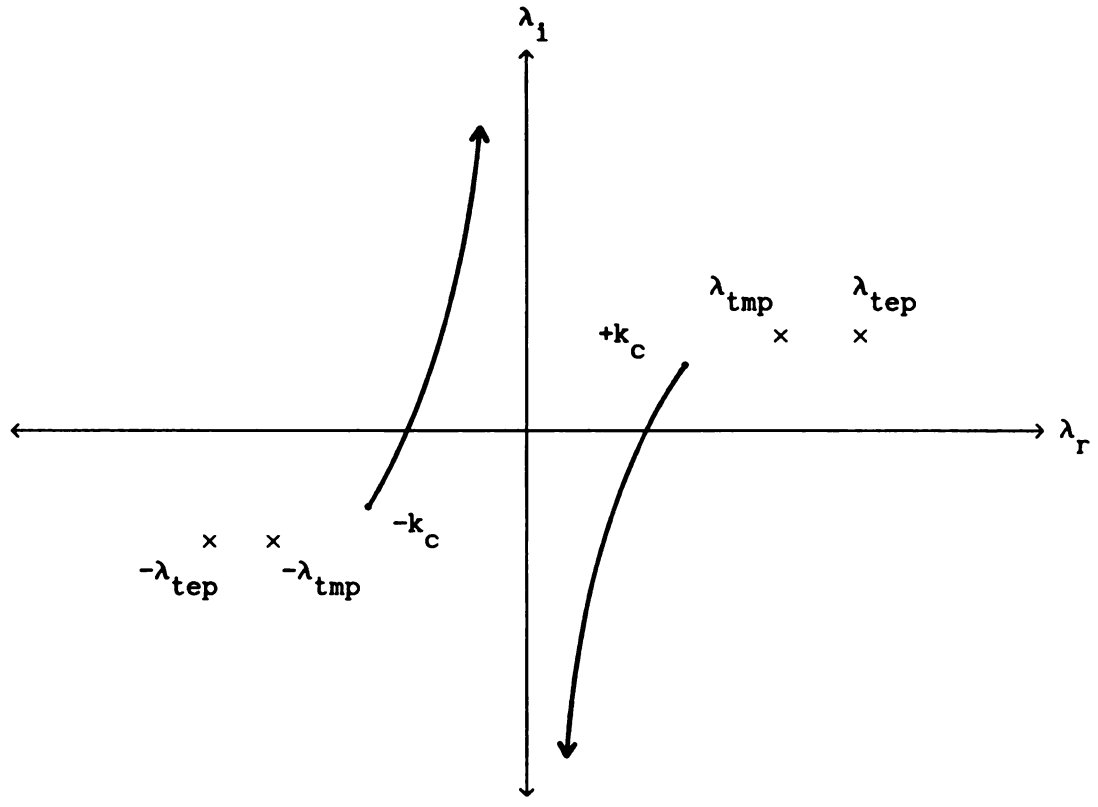

Figure 4. Migration of singularities across the λ_r axis.

Also, the curvature of the hyperbolic branch cuts (see Fig. 4) may be ignored. The justification for this approximation relies on the fact that the imaginary part of k_c is small and resides only slightly above the real axis.

The real line integration path specified in expression (34) must be slightly deformed above the real axis, as illustrated in Figure 5, so that it does not violate the migration paths of the singularities and render the integral undefined [1]. In order to evaluate spectral integral (34) with the path defined as in Figure 5, it is helpful to consider the path of integration illustrated in Figure 6. Since the integrand in expression (34) is analytic everywhere within the closed contour displayed in Figure 6, Cauchey's integral theorem may be applied leading to

$$I_{original} + I_{\infty} + I_{real} + I_{TE} + I_{TM} + I_{branch} = 0. \tag{36}$$

In the above relation, I denotes integration of expression (34) about corresponding portions C of the contour specified in Figure 6. In relation (36), $I_{\infty} \approx 0$ due to the nature of the integrand (see Appendix C); therefore, this result may be evaluated as

$$I_{original} = - I_{real} - I_{TE} - I_{TM} - I_{branch}. \tag{37}$$

As observed in expression (37), evaluation of eq. (34) with the original path of integration (Fig. 5) is equivalent to it's evaluation with the path of integration specified by the RHS of expression (37). The latter path (RHS) turns out to be numerically superior to the former path

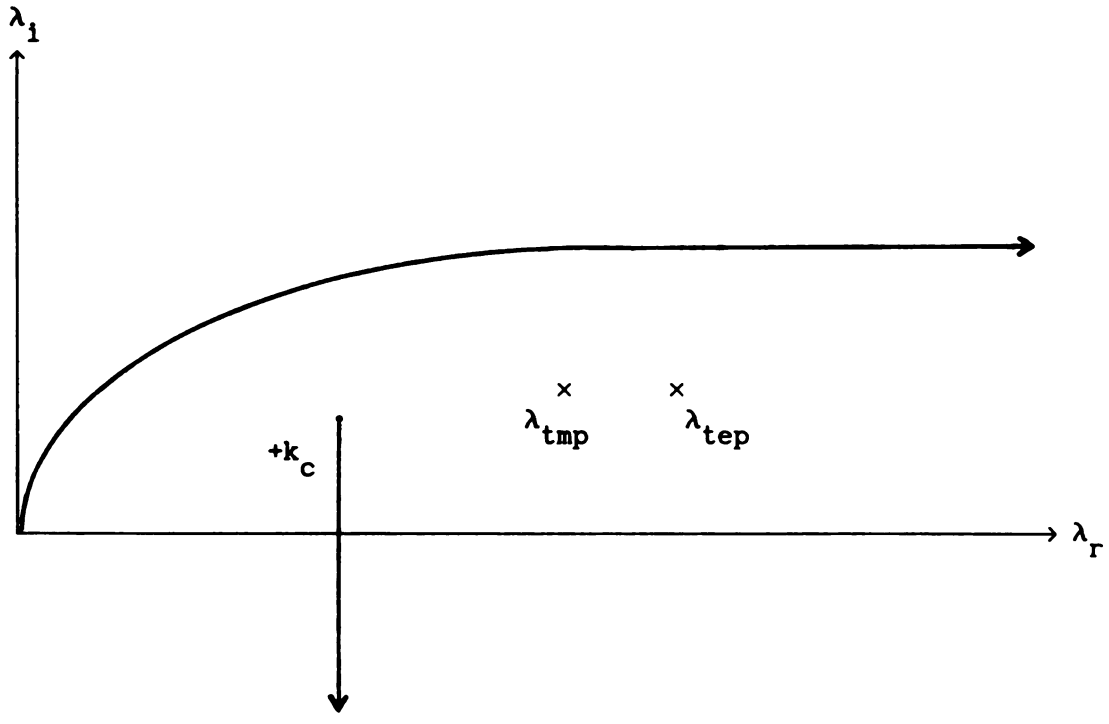

Figure 5. Correct path of integration.

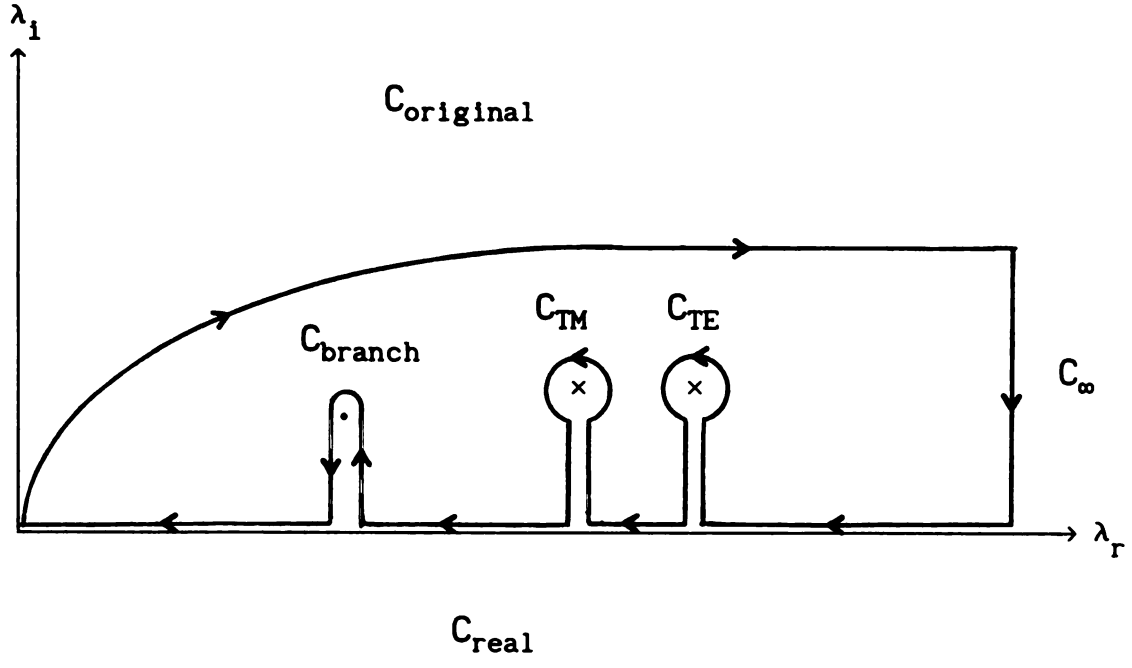

Figure 6. Deformed contour of integration.

(LHS). The reason being that the residues, resulting from I_{TE} and I_{TM}, can be analytically evaluated (refer to Appendix D) leaving only the real line integration and the branch cut integration for numerical evaluation. This greatly reduces the amount of numerics involving complex numbers.

The exact procedure employed in the present and the previous sections may be utilized to evaluate expression (35). The resulting path of integration obtained for spectral integral (35) is the same as in relation (37) with the exception of the TM pole contribution. This pole is of no consequence since it is not implicated in representation (35).

4.4.3 NUMERICAL RESULTS FOR RADIAL MODE

Numerical results may be pursued for both the radial and circumferential modes by numerically implementing eqs. (27) and (33), respectively. Although resonant frequencies can be obtained for the radial modes, none can be determined for the circumferential modes. The failure to determine resonant frequencies for these modes suggests that these modes may be purely evanescent, non-resonating modes [1].

A FORTRAN program provides a numerical solution to matrix eq. (27), yielding resonant frequencies for the radial modes. As stated earlier, non-trivial solutions to the matrix eq. require a vanishing determinant. This leads to a polynomial in the complex frequency ω, roots of which correspond to the various modes of resonance. These eigenvalues are searched for in the complex ω plane via secant method (which involves choice of an initial ω_o that must be in the near proximity of the desired resonant frequency). For numerical convenience the resonant film

wavenumber,

$$k_f a = \frac{\omega a}{c_f} \quad \text{where} \quad c_f = \frac{1}{\sqrt{\mu_o \varepsilon_f}}$$

is actually determined.

Computation of the matrix elements involved in calculating the determinant of eq. (27) is handled in several steps. First, for each iteration of the secant method, the location of any surface wave poles ($\lambda_p=\lambda_{pr}+j\lambda_{pi}$) present must be determined (for all results only the TM_o pole is excited). The surface wave poles lie near the λ_r axis in the region between $\lambda=k_c$ and $\lambda=k_f$ (refer to Fig. 6). (For the remainder of this section the cover wavenumber will be represented as $k_c=k_{cr}+jk_{ci}$.) A small region on the λ_r axis (of width 2ϵ centered about real part of the pole) is excluded and integrated analytically (see Appendix E) to avoid numerical overflow problems. Once the pole is determined, integration of the integrand in expression (34) along the intervals $\lambda=0$ to $\lambda=k_{cr}$ (C_{real}), $\lambda=k_{cr}$ to $\lambda=k_{ci}$ (C_{branch}), and $\lambda=k_{cr}$ to $\lambda=\lambda_{pr}-\epsilon$ (C_{real}) is handled numerically via Rhomberg integration. The integration of the integrand along the remaining interval, $\lambda=\lambda_{pr}+\epsilon$ to $\lambda=\infty$ (C_{real}), is numerically integrated step-by-step in full periods of oscillation of the integrand. Again, Rhomberg integration is used for each step in this last interval. Finally, analytic evaluation of the TM_o residue completes the computation of the matrix elements.

Figures 7-9 illustrate plots of the normalized resonant film wavenumber, $k_f a$, as a function of the normalized film thickness, t/a, for the lowest-order radial mode. In each figure, the permittivity of the cover is chosen to be that of free space. Film permittivities of $\varepsilon_f=1.1$

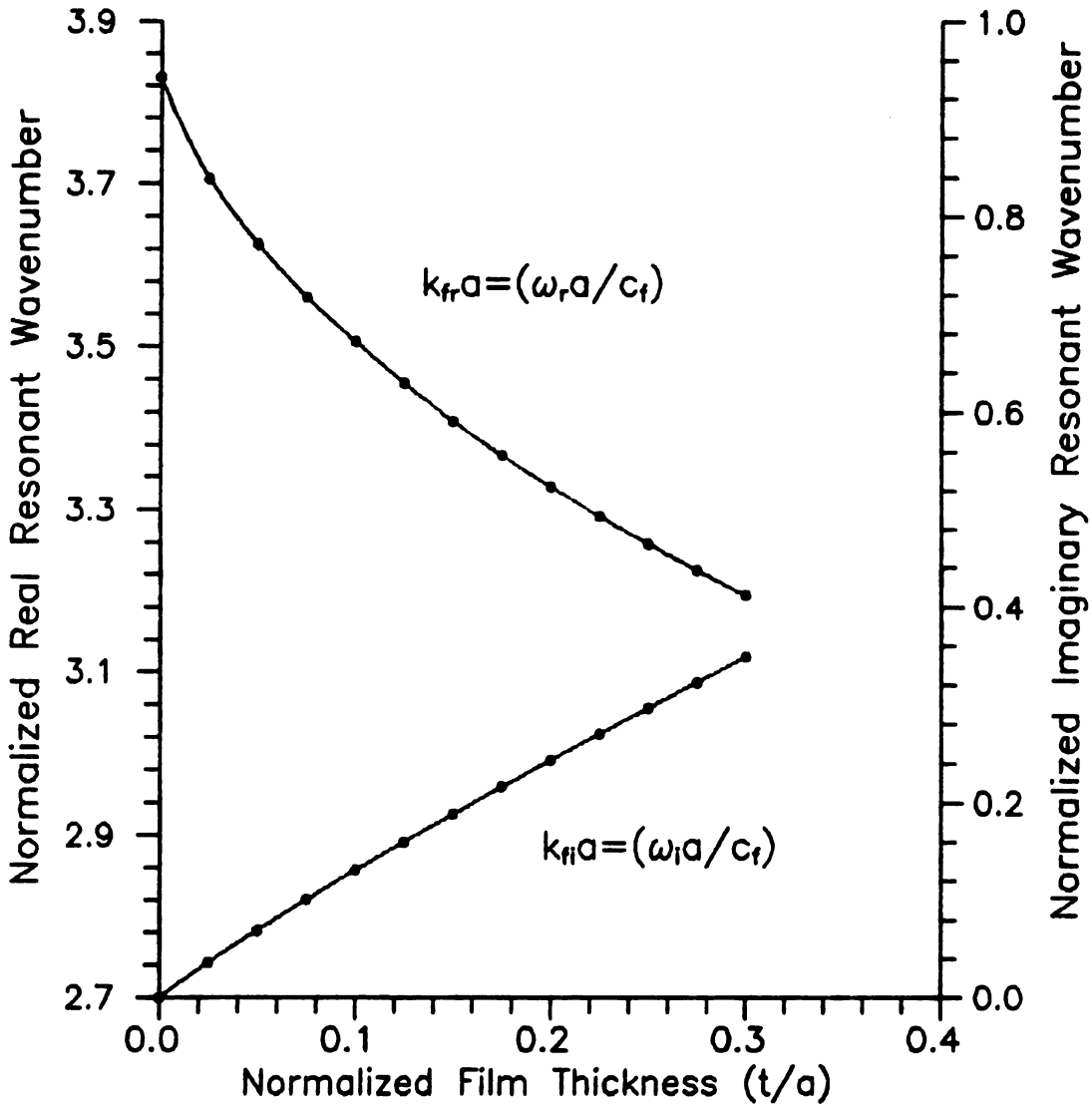

Figure 7. Normalized complex resonant wavenumber vs. normalized film thickness for the lowest order radial mode. (ε_c=1.0, ε_f=1.1)

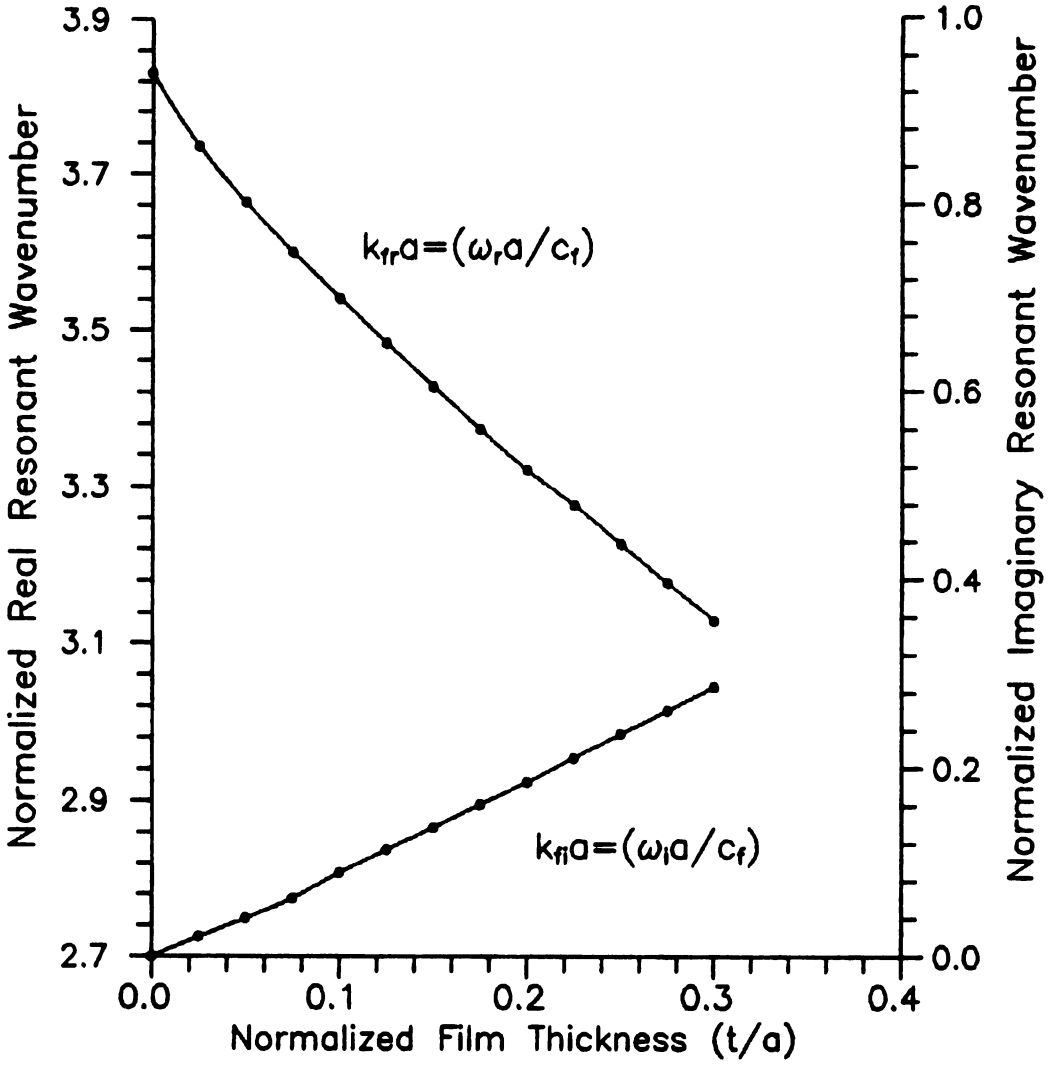

Figure 8. Normalized complex resonant wave-number vs. normalized film thickness for the lowest order radial mode. (ε_c=1.0, ε_f=2.65)

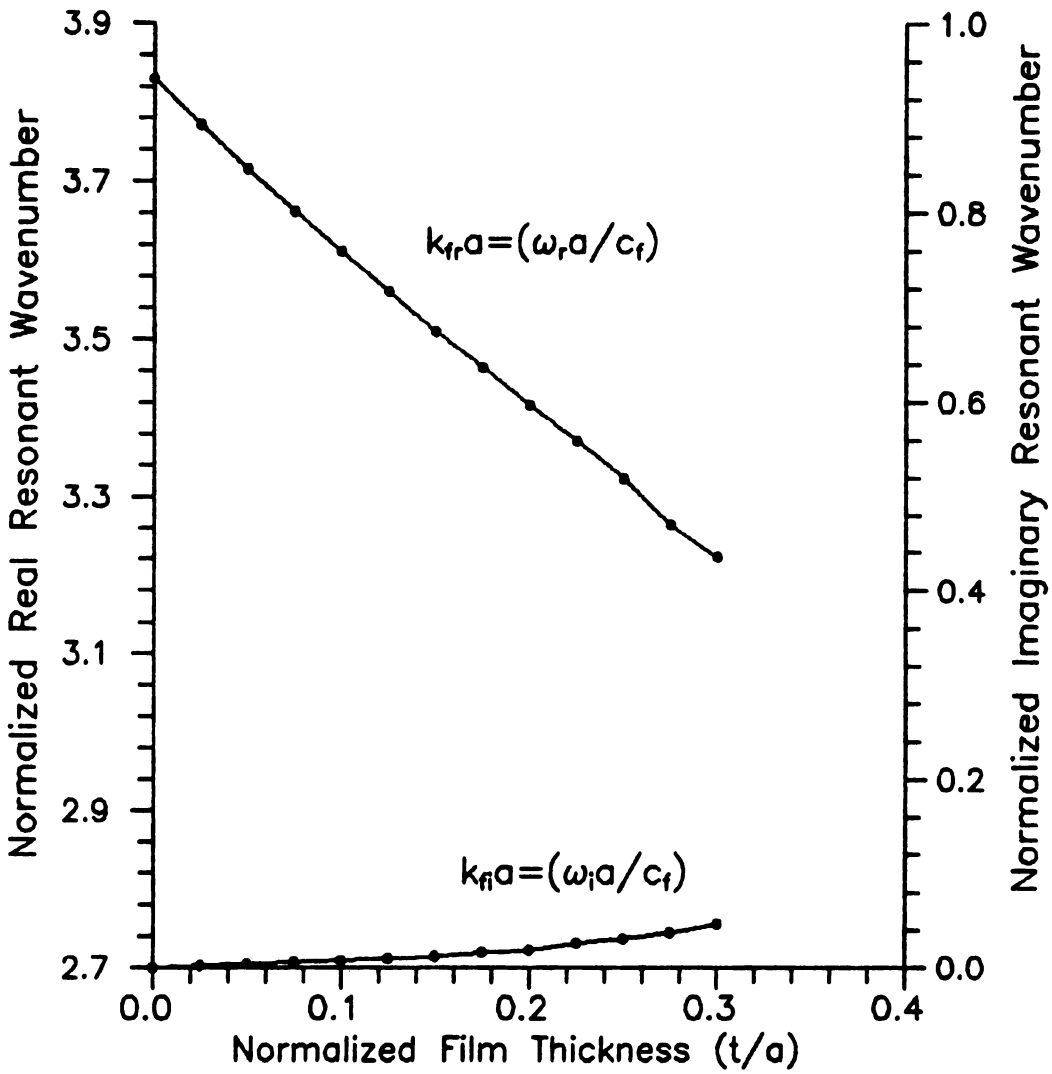

Figure 9. Normalized complex resonant wavenumber vs. normalized film thickness for the lowest order radial mode. ($\varepsilon_o=1.0$, $\varepsilon_f=9.6$)

(Fig. 7), ε_f=2.65 (Fig. 8), and ε_f=9.6 (Fig. 9) are also used. Further, three basis functions are found to be an adequate number for numerical convergence.

As expected, in each of the three plots, the real part of the resonant wavenumber ($k_{fr}a$) approaches the patch cavity [16] resonant wave number ($k_f a$=3.83) as the film thickness approaches zero. Also, the imaginary part of the resonant wavenumber ($k_{fi}a$), which corresponds to radiation, tends toward zero as the film thickness diminishes. For thicker film layers, though, the value of $k_{fr}a$ decreases appreciably from the value of $k_f a$ predicted by the simple patch theory. Also, for these thicker film layers, it is expected that fields residing underneath the patch will radiate more causing $k_{fi}a$ to increase. As observed from the plots, this is indeed true. When larger values of film permittivity are used as opposed to smaller values, the circular patch seems to radiate less provided the thickness remains fixed.

For the lowest-order mode, Figures 10-15 illustrate convergence plots of the normalized radial current magnitudes and corresponding phases as a function of the normalized radial coordinate (ρ/a) for the same three ε_f's used above. For each ε_f, two convergence plots are shown: one for a thin film layer (t/a=.025), and one for a thick film layer (t/a=.3). As observed from all the plots, it is clear that numerical convergence is in fact reached when three basis functions are used (as was assumed above). Also, for a given thickness, the current distributions for the various ε_f's seem to remain nearly the same.

Finally, for the lowest-order mode, comparisons of the normalized current magnitude determined from this analysis (IE solution) and the current predicted by the patch cavity model (which is given by $J_1(k_f a)$)

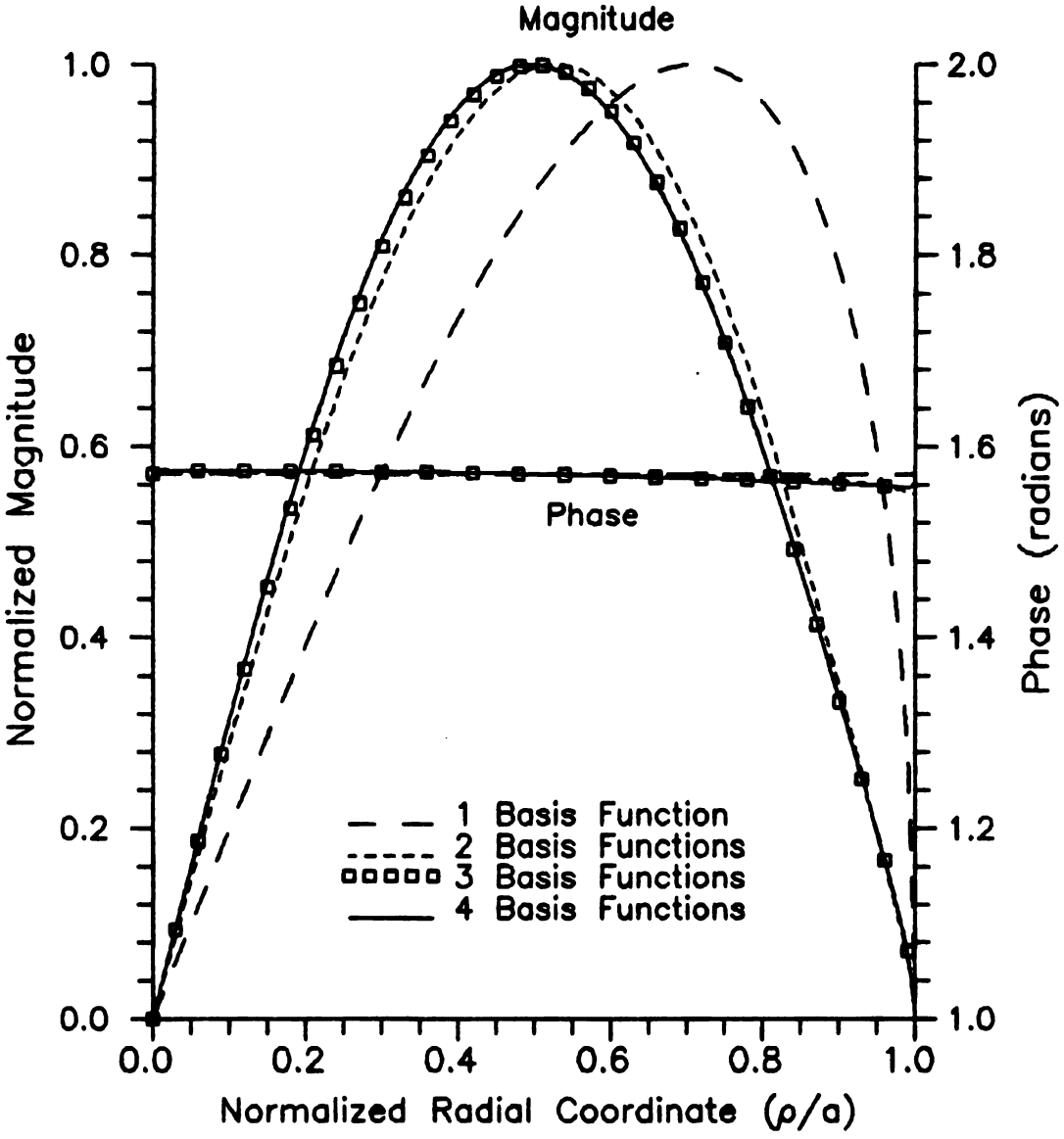

Figure 10. Current magnitude and phase vs. patch radial coordinate for lowest order radial mode (ε_c=1.0, ε_f=1.1, t/a=.025).

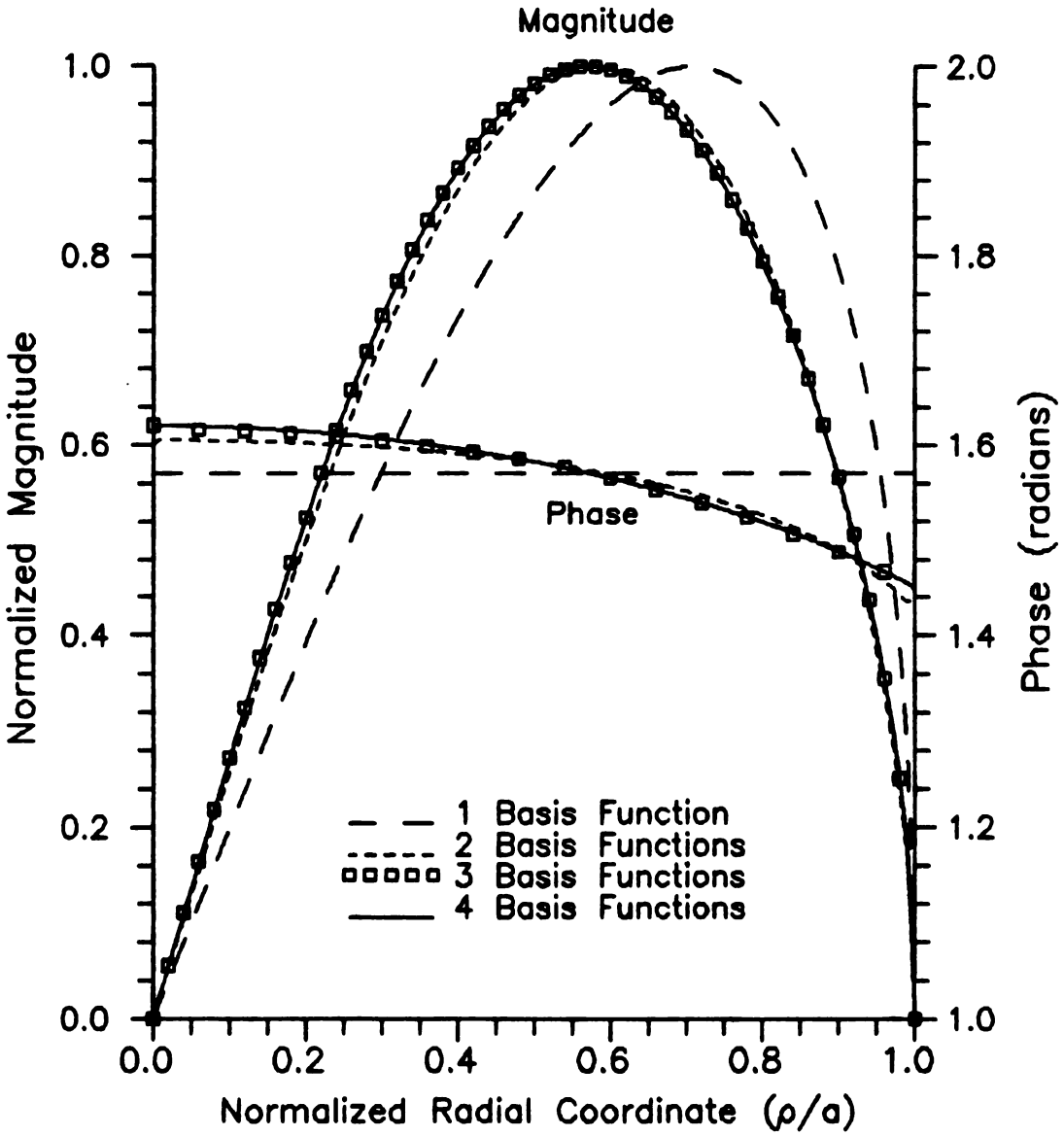

Figure 11. Current magnitude and phase vs. patch radial coordinate for lowest order radial mode (ε_c=1.0, ε_f=1.1, t/a=.3).

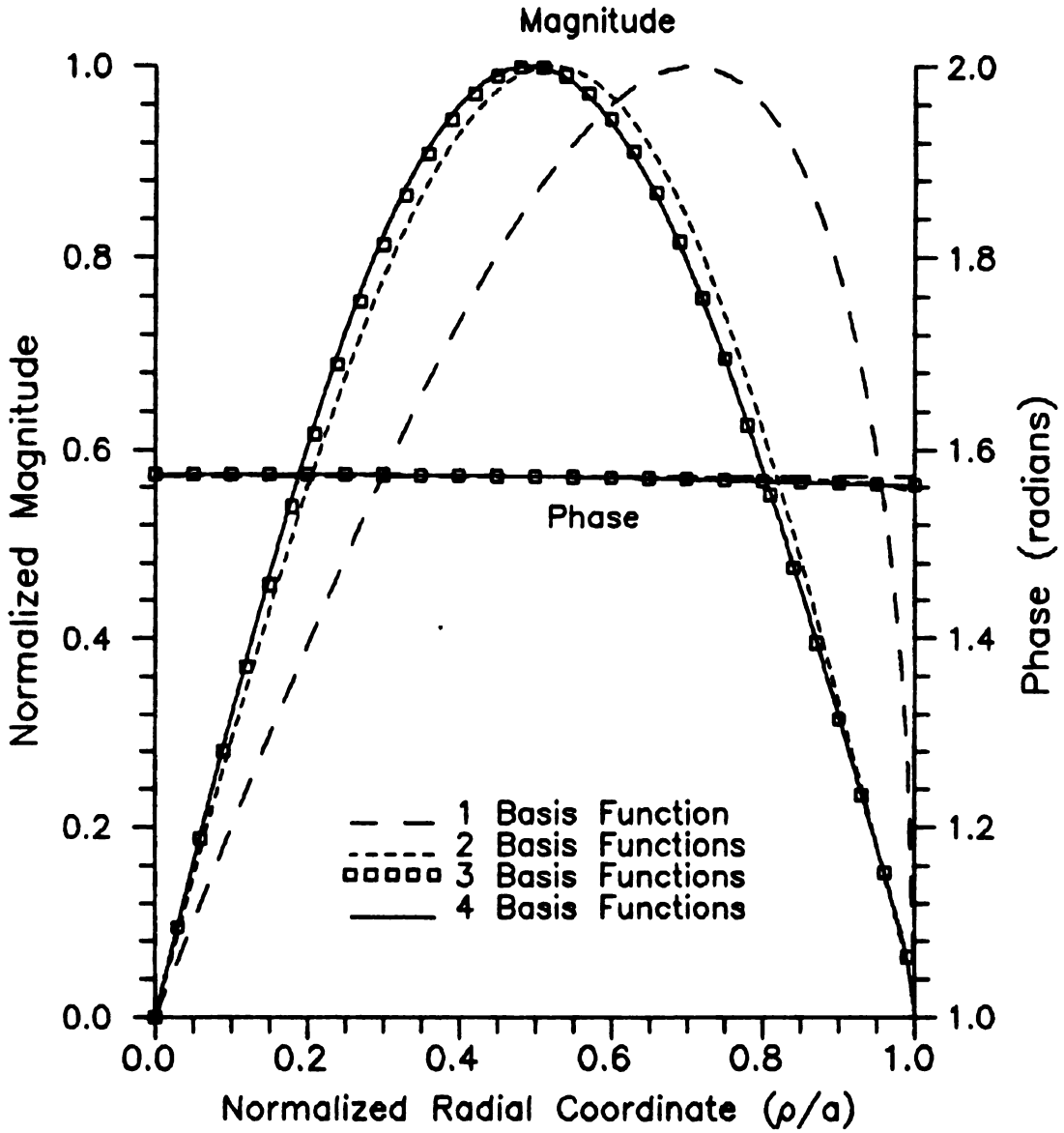

Figure 12. Current magnitude and phase vs. patch radial coordinate for lowest order radial mode (ε_c=1.0, ε_f=2.65, t/a=.025).

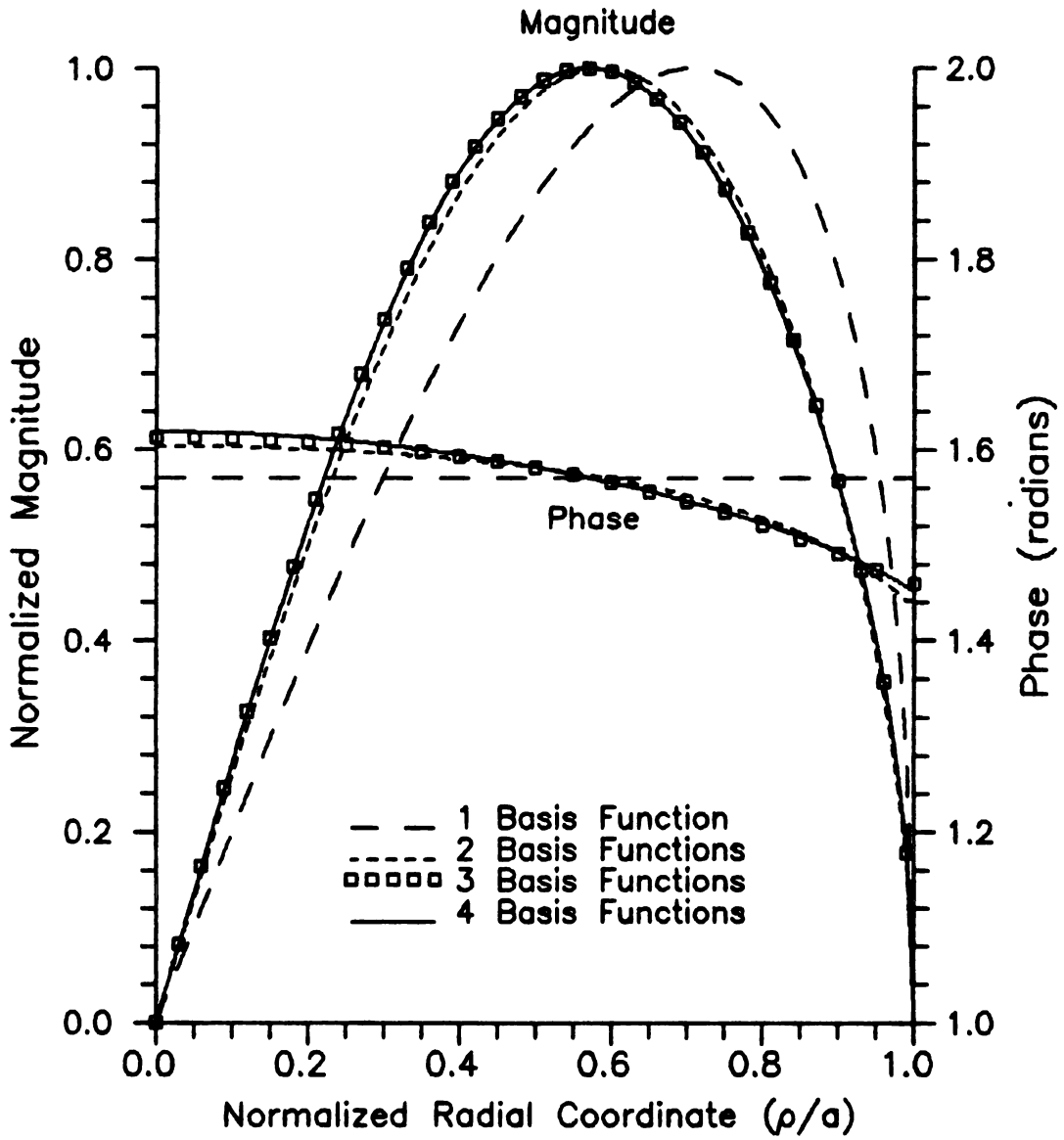

Figure 13. Current magnitude and phase vs. patch radial coordinate for lowest order radial mode (ε_c=1.0, ε_f=2.65, t/a=.3).

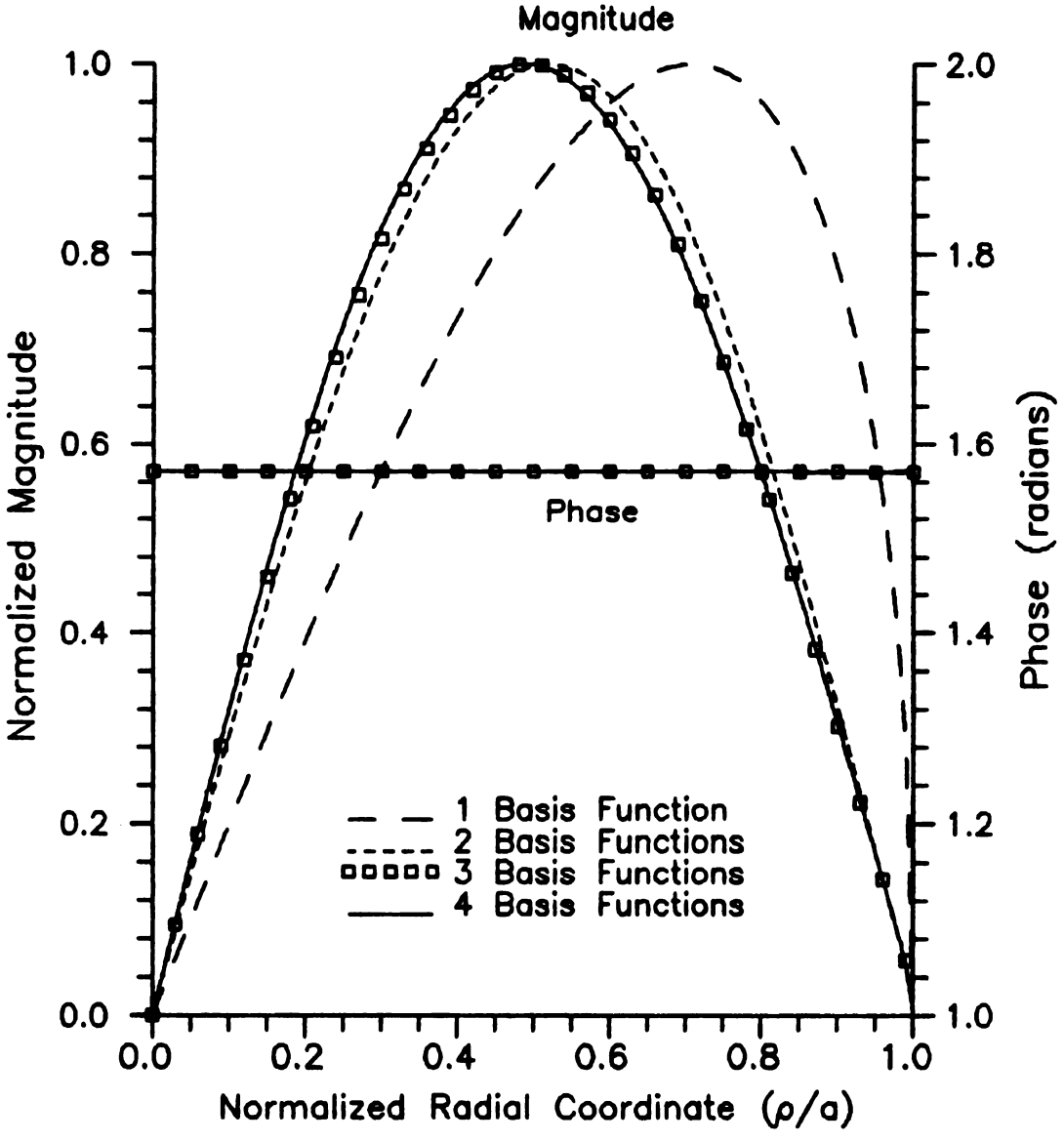

Figure 14. Current magnitude and phase vs. patch radial coordinate for lowest order radial mode (ε_c=1.0, ε_f=9.6, t/a=.025).

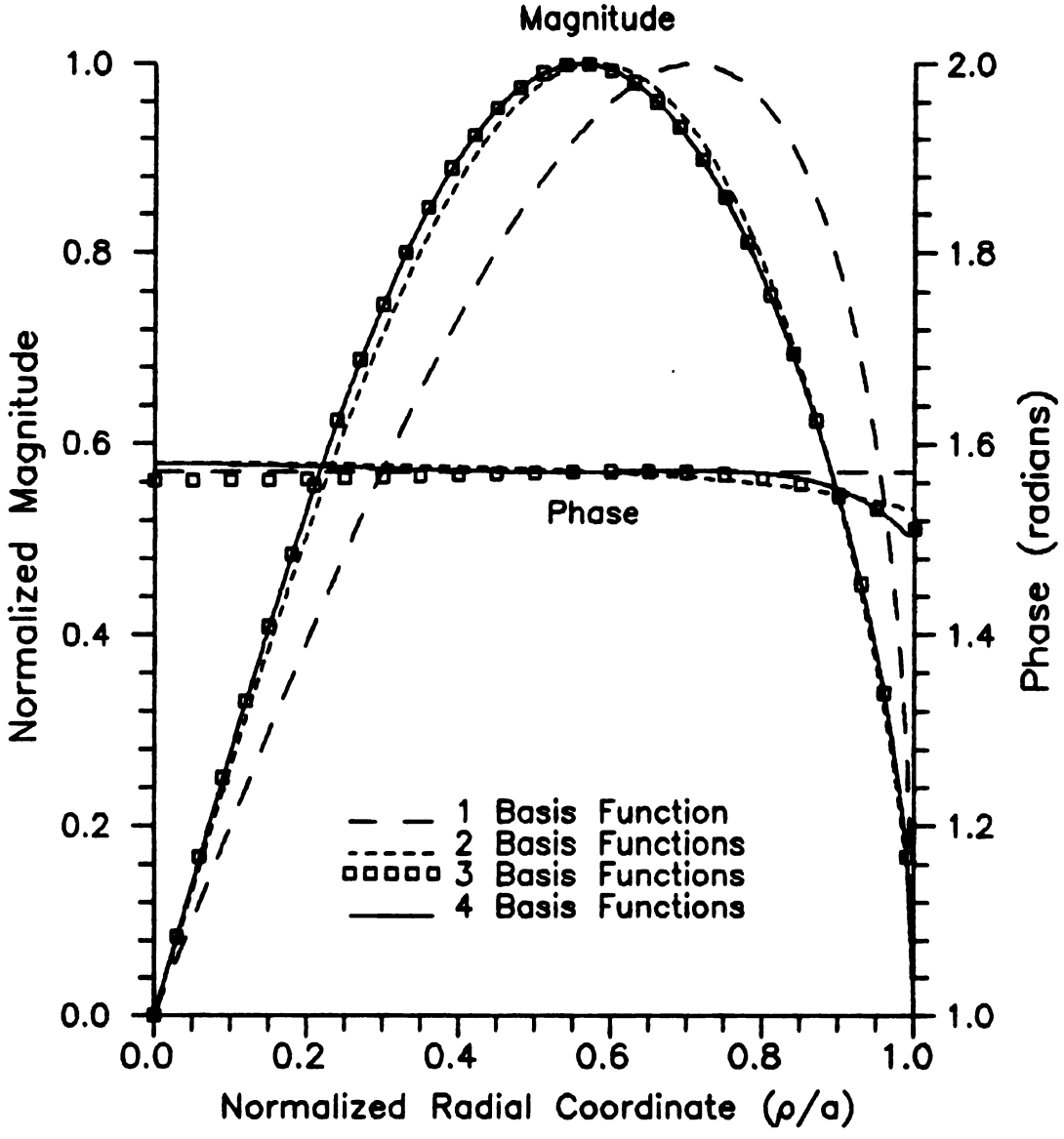

Figure 15. Current magnitude and phase vs. patch radial coordinate for lowest order radial mode (ε_c=1.0, ε_f=9.6, t/a=.3).

are made for thin and thick film layers. As seen from Figures 16 and 17, the patch cavity current is in good agreement with the current magnitude predicted by the IE solution when the film layer is thin, but the cavity current deviates appreciably from the IE solution current when the film layer is thick.

The remaining figures depict results for some of the higher-order modes. Figure 18 illustrates the resonant wavenumber as a function of film thickness for the first higher-order mode. For this higher mode, results converge well when five basis functions are used. Also, the resonant wavenumber plot for this mode displays similar trends to the wavenumber plots for the lowest-order mode. The current distribution shown in Figure 19 demonstrates that five basis functions are sufficient to yield numerical convergence for this higher-order mode. This seems reasonable since spatial oscillations of the current have increased. Figure 20 shows the current distribution for the second higher-order mode with $k_f a = 9.56 + j.269$. Again, five basis functions are used.

4.5 SUMMARY AND CONCLUSIONS

The coupled IE's for the resonant patch currents, developed in Chapter III, decouple for the case of n=0. These decoupled IE's, eqs. (4.13) and (4.14), describe axially symmetric resonant modes. IE (4.13) describes modes where the current sustained at resonance has only a radial component (radial modes). IE (4.14) describes modes where the resonant current has only an azimuthal component (circumferential modes).

Applying Galerkin's method to both IE's leads to the following two

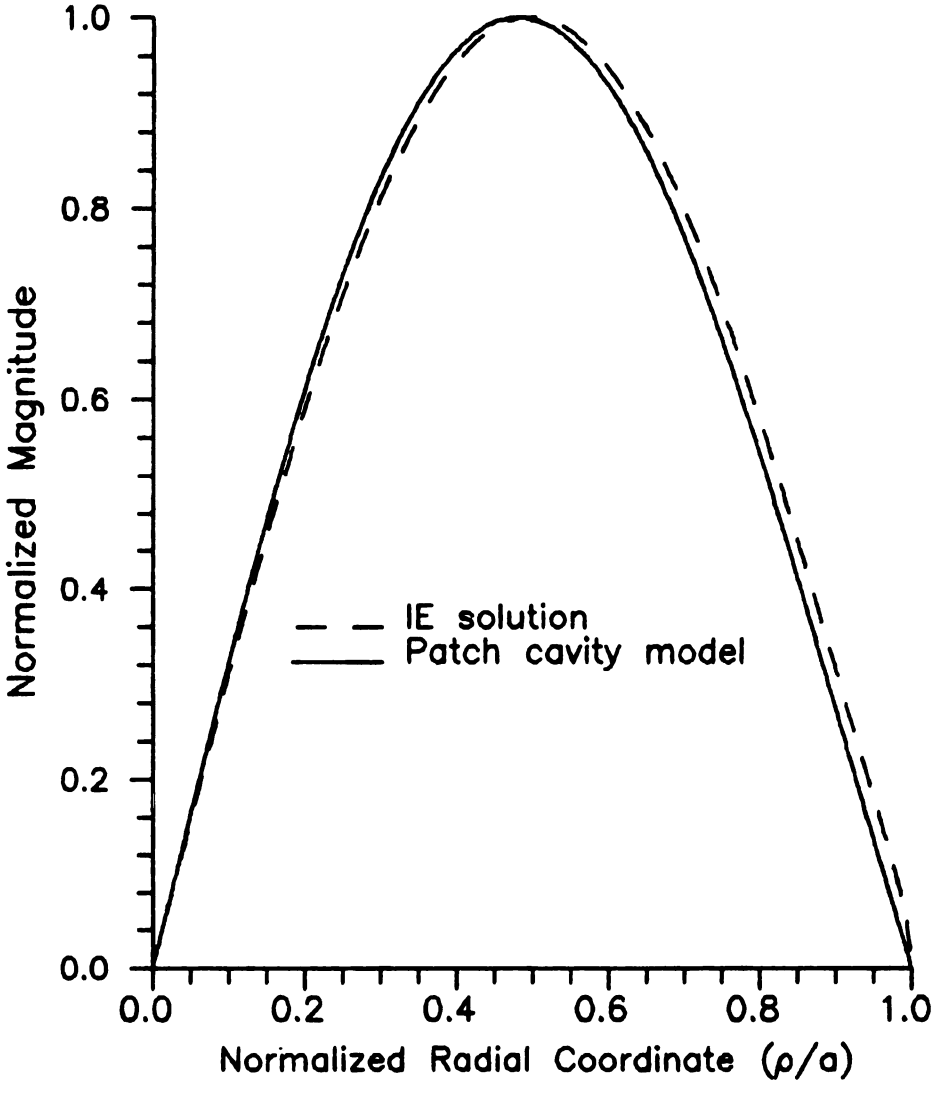

Figure 16. Current magnitude vs. patch radial coordinate for lowest order radial mode (ε_c=1.0, ε_f=2.65, t/a=.025).

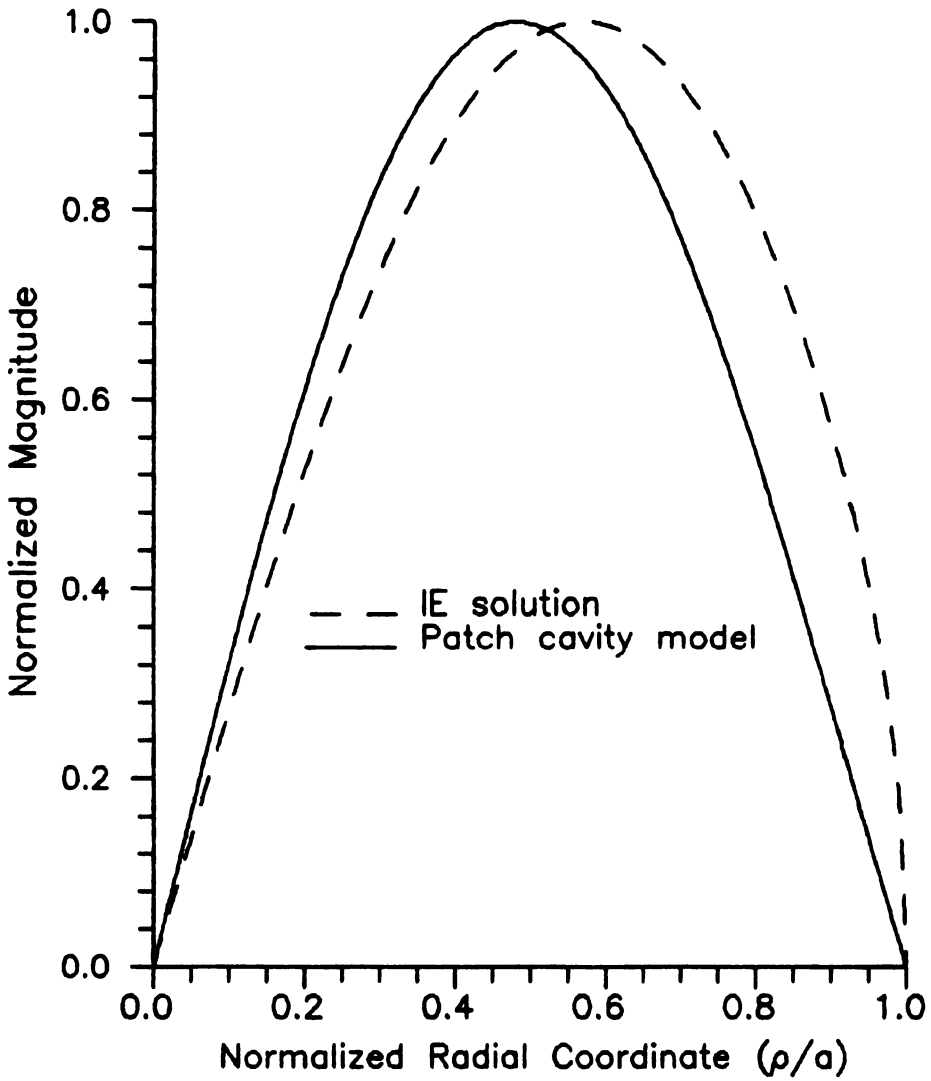

Figure 17. Current magnitude vs. patch radial coordinate for lowest order radial mode (ε_c=1.0, ε_f=2.65, t/a=.3).

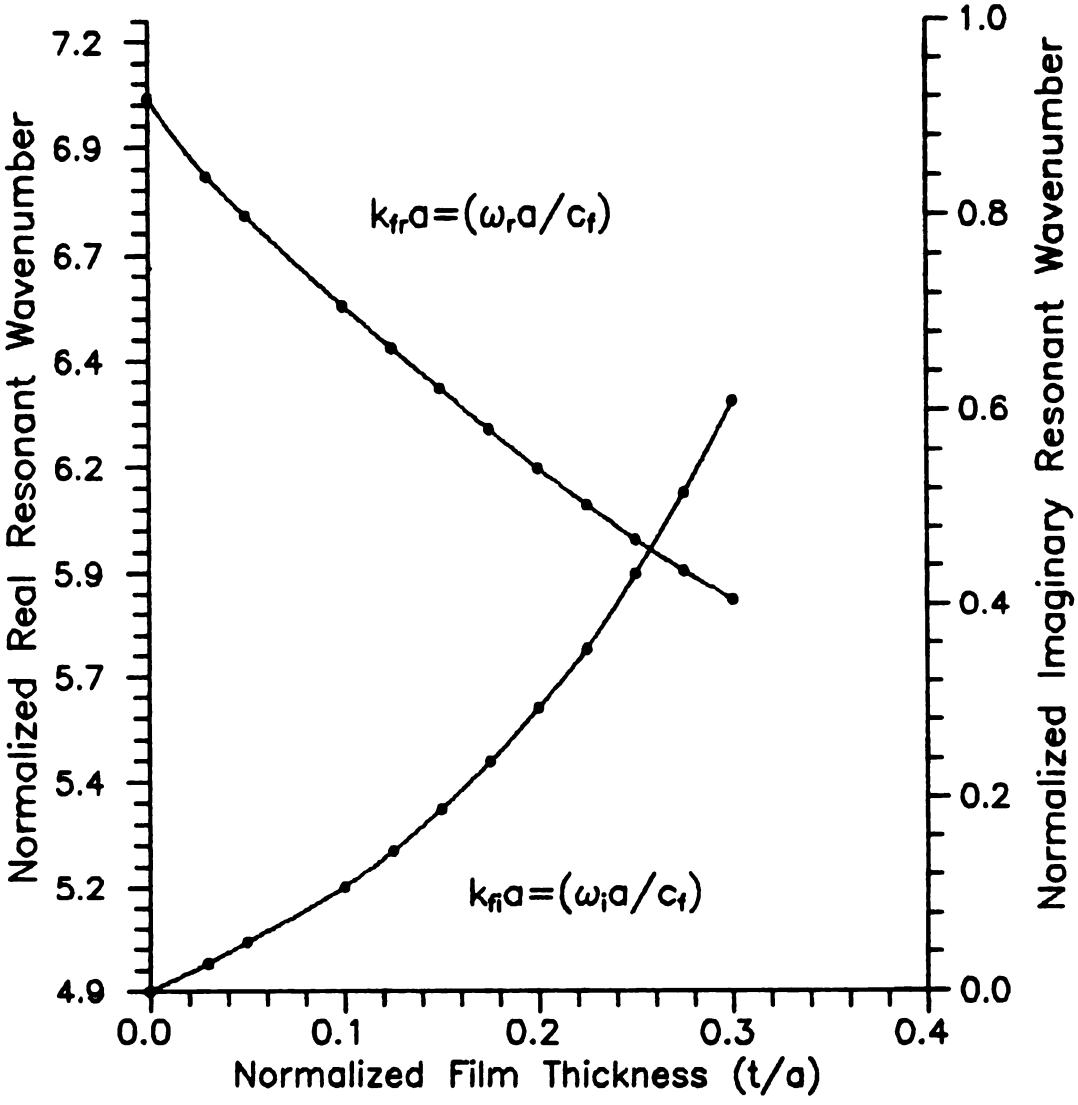

Figure 18. Normalized complex resonant wave-number vs. normalized film thickness for the first higher order radial mode. (ε_c=1.0, ε_f=2.65)

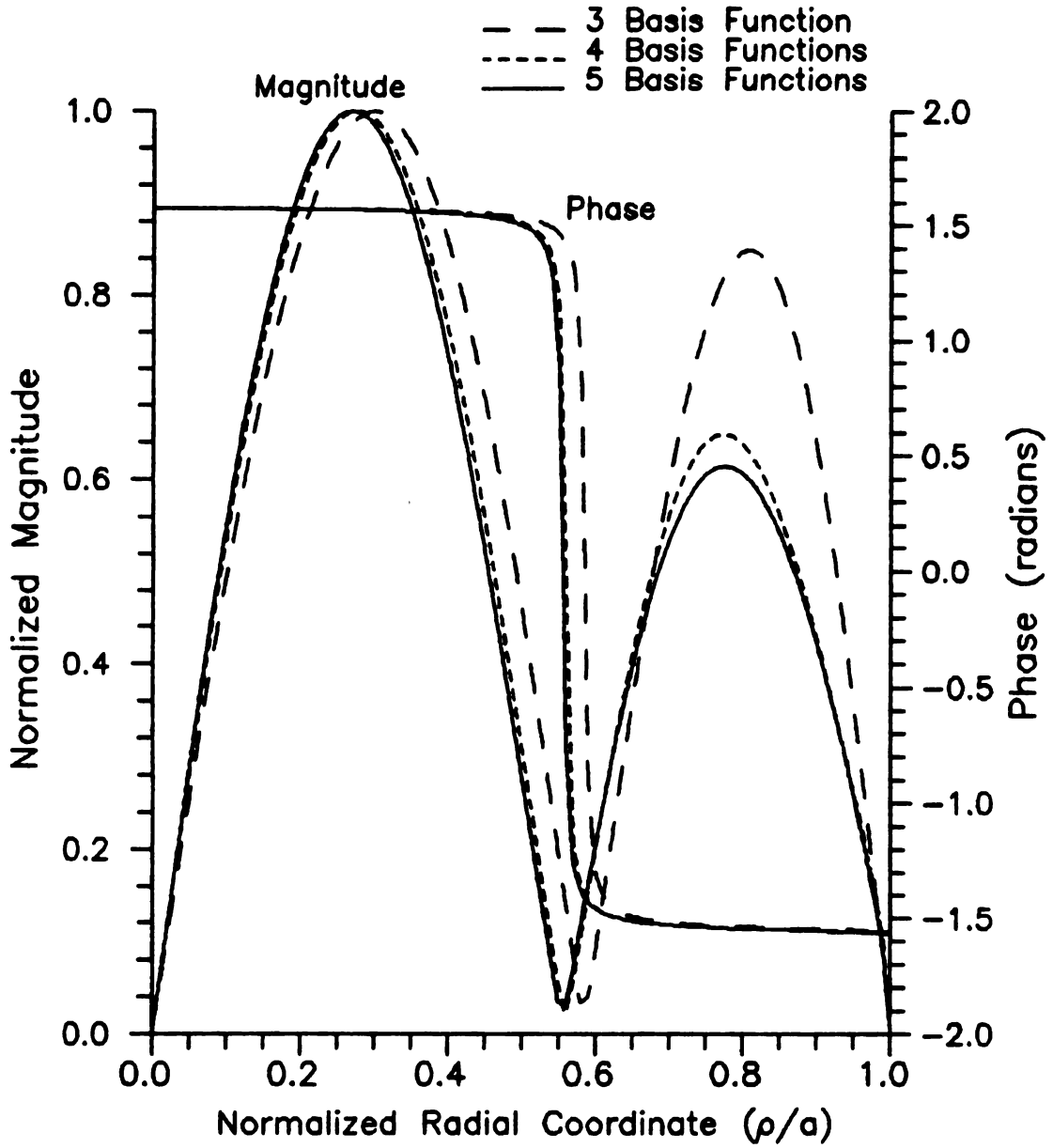

Figure 19. Current magnitude and phase vs. patch radial coordinate for first higher order radial mode (ε_c=1.0, ε_f=2.65, t/a=.03).

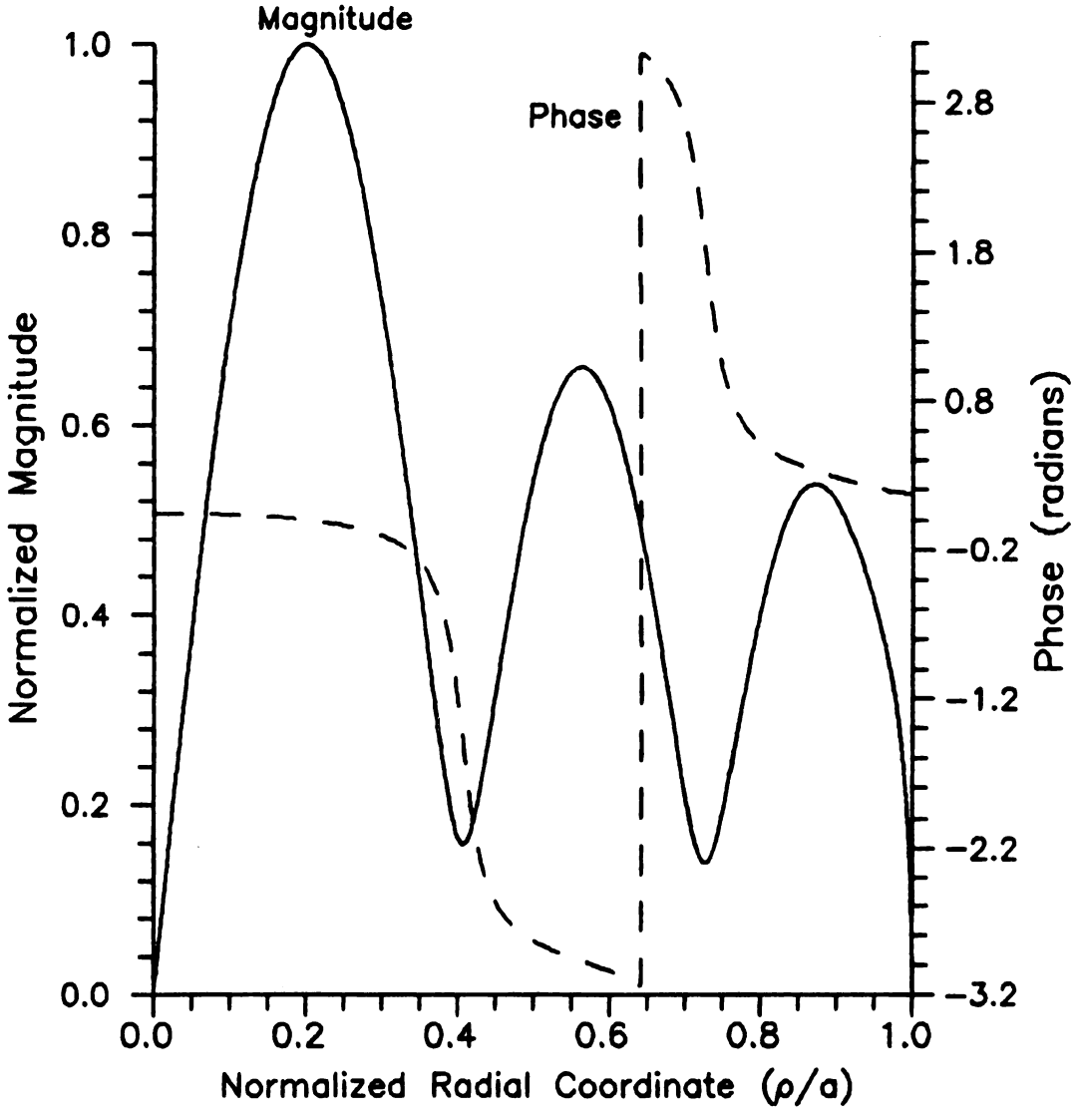

Figure 20. Current magnitude and phase vs. patch radial coordinate for second higher order radial mode (ε_c=1.0, ε_f=2.65, t/a=.1).

homogeneous matrix equations

$$\sum_{m=0}^{N} A_{\rho m} B_{lm} = 0 \qquad l = 0,1,2,\ldots,N \tag{4.27}$$

$$\sum_{m=0}^{N} A_{\theta m} C_{lm} = 0 \qquad l = 0,1,2,\ldots,N \tag{4.32}$$

from which the resonant frequencies and current distributions for the two types of modes may be obtained. Each matrix element of eqs. (4.27) and (4.32) contain spectral inversion integrals, given as

$$B_{lm} = \int_0^{\infty} \left[\frac{(k_c^2 - \lambda^2)\lambda}{Z^h(\lambda)} + \frac{\lambda^3 (N_{fc}^2 - 1)}{Z^h(\lambda) Z^e(\lambda)} \right] \tilde{J}_l(\lambda a) \tilde{J}_m(\lambda a)\, d\lambda \tag{4.34}$$

$$C_{lm} = \int_0^{\infty} \frac{\lambda}{Z^h(\lambda)} \hat{J}_l(\lambda a) \hat{J}_m(\lambda a)\, d\lambda \tag{4.35}$$

that must be evaluated when solving these matrix equations. The proper path of integration for matrix elements (4.34) and (4.35) relies on the location of the surface wave poles and the correct choice of the branch cut implied by the wavenumber parameter

$$p_c = \sqrt{\lambda - k_c}\,\sqrt{\lambda + k_c}.$$

Imposing the physical constraint of a lossy cover region (with $k_c = k_c' - jk_c''$ and $k_c'' > 0$) which supports decaying outward propagating waves, leads to the standard hyperbolic branch cuts emanating downward from

$\lambda=+k_c$ and upward from $\lambda=-k_c$ (refer to Fig. 3). But for temporal resonance, k_c'' becomes positive, and in order to sustain a continuous transition, the branch cuts and pole singularities "migrate" across the real axis; therefore, the path of integration must be deformed so that it does not violate the "migration" paths of the singularities (refer to Fig. 5).

Once the correct integration paths are chosen, eqs. (4.27) and (4.32) are implemented numerically. The solutions to eq. (4.26) (radial modes) yield reasonable resonant frequencies and current distributions. Resonant frequencies for the circumferential modes, however, can not be determined. This leads to the conclusion that there exists no pole singularities corresponding to such modes.

The previously described determination of the branch cuts and integration contours for spectral integral (4.34) yields reasonable results but is somewhat contrived. A more rigorous explanation may result from investigation of the forward transforms of the potential functions used in the derivation of the resonant IE's described in Chapter III. For example, the spatial scalar representation of the principal Green's function from Chapter II, given as

$$G^p(\vec{r}|\vec{r}') = \frac{e^{-jk_c|\vec{r}-\vec{r}'|}}{4\pi|\vec{r}-\vec{r}'|}$$

may be Fourier transformed in the transverse directions ($\hat{x}$ and $\hat{z}$ directions) as

$$\tilde{G}^{p}(\xi,\zeta,y) = \int_{-\infty}^{\infty}\int \frac{e^{-jk_c|\vec{r}-\vec{r}'|}}{4\pi|\vec{r}-\vec{r}'|} e^{-j(\xi x + \zeta z)}\, dxdz.$$

For resonance, it has already been observed that $k_c=k_c'+jk_c''$. This allows the above transform to be expressed as

$$\tilde{G}^{p}(\xi,\zeta,y) = \int_{-\infty}^{\infty}\int \frac{e^{-jk_c'|\vec{r}-\vec{r}'|}}{4\pi|\vec{r}-\vec{r}'|} e^{+k_c''|\vec{r}-\vec{r}'|} e^{-j(\xi x + \zeta z)}\, dxdz.$$

It is obvious from the above expression that the forward transform of the principle Green's function does not converge due to the growing exponential factor. It is conjectured that if convergence of the above forward transform is satisfied, the correct intrgration path will automatically be determined when the inverse transform is taken. This argument may be extended to all the potential functions (since they have similar propagation characteristics), in turn, avoiding the previous difficulties of determining the correct branch cuts and integration paths.

CHAPTER V

CONCLUSIONS AND RECOMMENDATIONS

Integral-operator techniques provide a conceptually exact description of resonant structures in an integrated circuit environment. Unlike most other techniques, the EFIE approach allows for the accurate determination of complex resonant frequencies, which include the effect of radiation damping. This technique proves useful for the analysis of a circular patch resonator within the integrated conductor/film/cover environment.

Chapter two pursued a somewhat general analysis of a arbitrary resonant structure within the integrated environment. A detailed discussion of the electric Green's dyad for the tri-layered medium was reviewed. Application of this dyad lead to a homogeneous IE describing the natural resonance of the structure.

In chapters three and four, the previous Green's dyad was appropriately represented in polar form, enabling it's convenient application to a circular patch. This lead to the development of two coupled homogeneous IE's describing the various modes of resonance for the patch. These IE's provided analytic angular mode indexing. For the lowest-order angular mode, the IE's decoupled leading to independent IE's describing axially-symmetric resonant modes. Galerikin's method with Tchebychev polynomials lead to successful numeric determination of resonant frequencies and current distributions for the radial modes. Investigation of the solution for the first higher-order angular mode,

which corresponds to the dominant resonant mode of the circular patch, is encouraged.

Also, in chapter four it was observed that numeric solution for the resonant frequencies involved evaluation of spectral inversion integrals. Due to the nature of the resonant structure, determination of the correct integration path for these integrals became complicated and lacked a rigorous approach. (Identical problems have also been confronted in determining the leaky modes of an infinite microstrip waveguiding structure.) A rigorous determination of the aforementioned integration path is a topic of research strongly encouraged.

APPENDICES

APPENDIX A

APPENDIX A

REPRESENTATION FOR J_0 VIA SUMMATION THEOREM

The zeroth order Bessel function evident in expressions (3.7a) and (3.7b),

$$J_o(\lambda|\vec{\rho}-\vec{\rho}'|) = J_o(\sqrt{\rho^2 + \rho'^2 - 2\rho\rho'\cos(u)}) \tag{A1}$$

may be conveniently expressed by invoking the "summation theorem" for Bessel functions [13]. This theorem is briefly stated as

$$e^{j\nu\psi}Z_\nu(mR) = \sum_{k=-\infty}^{\infty} J_k(m\rho)Z_{\nu+k}(mr)e^{jk\phi}$$

where

$$r > 0,\ \rho > 0,\ \phi > 0$$

$$R = \sqrt{r^2 + \rho^2 - 2\rho\rho'\cos(u)}$$

$$\rho < r, \quad \text{and} \quad 0 < \psi < \frac{\pi}{2}.$$

The quantities r, ρ, and R can be considered the sides of a triangle such that the angle between the sides r and ρ is equal to ϕ, and the angle opposite side ρ is equal to ψ. With the specializations

$$Z_\nu = J_\nu,\ \nu = 0,\ m = \lambda,\ \phi = u,$$

and $R = |\vec{\rho}-\vec{\rho}'| = \sqrt{\rho^2 + \rho'^2 - 2\rho\rho'\cos(u)}$

$J_o(\lambda|\vec{\rho}-\vec{\rho}'|)$ may be written as

$$J_o(\lambda|\vec{\rho}-\vec{\rho}'|) = \sum_{k=-\infty}^{\infty} J_k(\lambda\rho)J_k(\lambda\rho')e^{jku}. \qquad (A2)$$

Finally, by rewriting the exponential and utilizing the relation $J_{-n}(z) = (-1)^n J_n(z)$ [10], eq. (A2) may be ultimately expressed as

$$J_o(\lambda|\vec{\rho}-\vec{\rho}'|) = J_o(\lambda\rho)J_o(\lambda\rho') + \sum_{k=1}^{\infty} J_k(\lambda\rho)J_k(\lambda\rho')\cos(u)$$

where the restriction $\rho'<\rho$ ($\rho<r$) is no longer necessary. This expression for $J_o(\lambda|\vec{\rho}-\vec{\rho}'|)$ was implemented in modifying eq. (3.7b) to eq. (3.8).

APPENDIX B

APPENDIX B

TCHEBYCHEV RECURRENCE RELATION

The recursion relation,

$$2uT_n(u) = T_{n-1}(u) + T_{n+1}(u) \tag{B1}$$

presented in section 4.3.1, introduces a potential problem for values of n less than or equal to zero. For example, when n=0, n-1 becomes negative, but Tchebychev polynomials are not defined for negative orders. If this recursion relation is to be valid when negative orders are implied, the following constraint must be imposed:

$$T_n(u) = T_{|n|}(u) \quad \text{for } n = -1, -2, \ldots \quad [12] \tag{B2}$$

When restriction (B2) is implemented, the recursion relation produces valid results for all integer values of n.

Using recursion relation (B1) along with restriction (B2) allows the term $u(1 - u^2)T_{2m+1}(u)$, evident in eq. (4.21), to be conveniently expressed. From this term it is evident that the quantities $uT_{2m+1}(u)$ and $u^3T_{2m+1}(u)$ must be determined. Applying relation (B1) leads to

$$uT_{2m+1}(u) = \frac{1}{2}\left[T_{2m}(u) + T_{2m+2}(u)\right] \tag{B3}$$

$$u^2T_{2m+1}(u) = \frac{1}{4}\left[T_{2m-1}(u) + 2T_{2m+1}(u) + T_{2m+3}(u)\right]$$

$$u^3 T_{2m+1}(u) = \frac{1}{8}\left[T_{2m-2}(u) + 3T_{2m}(u) + 3T_{2m+2}(u) + T_{2m+4}(u)\right] \qquad \text{(B4)}$$

Combining expressions (B3) and (B4) yields

$$u(1 - u^2)T_{2m+1}(u) = \frac{1}{8}\left[T_{2m}(u) + T_{2m+2}(u) - T_{2m-2}(u) - T_{2m+4}(u)\right] \qquad \text{(B5)}$$

It is observed that since expansion (4.19) begins with m=0, the order of the Tchebychev in the third term of eq. (B5) may become negative; therefore, restriction (B2) must be imposed leading to

$$u(1 - u^2)T_{2m+1}(u) = \frac{1}{8}\left[T_{2m}(u) + T_{2m+2}(u) + T_{|2m-2|}(u) + T_{2m+4}(u)\right]. \qquad \text{(B6)}$$

Expression (B6) is identical result presented by expression (4.22).

APPENDIX C

APPENDIX C

ASYMPTOTIC BEHAVIOR OF THE SPECTRAL INTEGRALS

For the radial mode, the matrix elements are given by expression (4.34) as

$$B_{lm} = \int_0^\infty \left[\frac{(k_c^2 - \lambda^2)\lambda}{Z^h(\lambda)} + \frac{\lambda^3(N_{fc}^2 - 1)p_c}{Z^h(\lambda)Z^e(\lambda)} \right] \tilde{J}_l(\lambda a)\tilde{J}_m(\lambda a)\, d\lambda. \qquad (4.34)$$

By considering the behavior of the above integrand for large values of λ, the following approximations may be made:

$$(k_c^2 - \lambda^2)\lambda \approx -\lambda^3$$

$$p_l = \sqrt{\lambda^2 - k_l^2} \approx \lambda$$

$$Z^h(\lambda) = p_c + p_f \coth(p_f t) \approx 2\lambda$$

$$Z^e(\lambda) = N_{fc}^2 p_c + p_f \tanh(p_f t) \approx \lambda(N_{fc}^2 + 1).$$

Also, with the assistance of the asymptotic expansion of Bessel functions J_ν with large argument, given by

$$J_\nu(z) \approx \sqrt{2/(\pi z)}\, \cos(z - \frac{\pi\nu}{2} - \frac{\pi}{4}) \qquad ([10],\ p.\ 364) \qquad (C1)$$

(z represents a complex quantity) the terms $\tilde{J}_l$ and $\tilde{J}_m$ may be approximated as

$$\tilde{J}_l(\lambda a) \approx \frac{1}{\lambda} \text{ (sin and cos terms)}$$

$$\tilde{J}_m(\lambda a) \approx \frac{1}{\lambda} \text{ (sin and cos terms).}$$

Utilizing all the previous approximations, it is observed that the integrand of expression (4.34) has the following non-convergent asymptotic behavior for large λ:

$$I_a \approx \frac{-1}{(N_{fc}^2 + 1)} \text{ (sin and cos terms).}$$

With this type of behavior it appears that the integral implicated by (4.34) is divergent. This is not the case, though. A more detailed inspection of $\tilde{J}_l$ and $\tilde{J}_m$ illustrates that the integral does converge.

The terms $\tilde{J}_l$ and $\tilde{J}_m$ assume the following generic form:

$$\tilde{J}_p(z) = \left[J_{\frac{1+2p}{2}}(z)\, J_{\frac{1-2p}{2}}(z) + J_{\frac{2p+3}{2}}(z)\, J_{\frac{-2p-1}{2}}(z) \right.$$

$$\left. - J_{\frac{1+|2p-2|}{2}}(z)\, J_{\frac{1-|2p-2|}{2}}(z) - J_{\frac{2p+5}{2}}(z)\, J_{\frac{-2p-3}{2}}(z) \right] \qquad \text{(C2)}$$

where $p=l,m$. Considering z large in the first term and applying relation (C1) leads to

$$J_{\frac{1+2p}{2}}(z)\, J_{\frac{1-2p}{2}}(z) \approx \frac{2}{\pi z} \cos\left(z - \frac{\pi}{2}\left(\frac{1+2p}{2}\right) - \frac{\pi}{4}\right) \cos\left(z - \frac{\pi}{2}\left(\frac{1-2p}{2}\right) - \frac{\pi}{4}\right)$$

$$= \frac{2}{\pi z} \sin\left(z - \frac{\pi p}{2}\right) \sin\left(z + \frac{\pi p}{2}\right). \qquad \text{(C3)}$$

Similarly, for z large the second, third, and fourth terms become

$$J_{\frac{2p+3}{2}}(z)\, J_{\frac{-2p-1}{2}}(z) \approx -\frac{2}{\pi z}\cos\left(z+\frac{\pi p}{2}\right)\cos\left(z-\frac{\pi p}{2}\right) \tag{C4}$$

$$J_{\frac{1+|2p-2|}{2}}(z)\, J_{\frac{1-|2p-2|}{2}}(z) \approx \frac{2}{\pi z}\sin\left(z-\frac{\pi}{4}|2p-2|\right)\sin\left(z+\frac{\pi}{4}|2p-2|\right) \tag{C5}$$

$$J_{\frac{2p+5}{2}}(z)\, J_{\frac{-2p-3}{2}}(z) \approx \frac{2}{\pi z}\sin\left(z-\frac{\pi p}{2}\right)\sin\left(z+\frac{\pi p}{2}\right). \tag{C6}$$

Utilizing expressions (C3)-(C6), relation (C2) may be rewritten for large z as

$$\tilde{J}_p(z) \approx \frac{-2}{\pi z}\left[\cos\left(z+\frac{\pi p}{2}\right)\cos\left(z-\frac{\pi p}{2}\right) + \sin\left(z-\frac{\pi}{4}|2p-2|\right)\sin\left(z+\frac{\pi}{4}|2p-2|\right)\right].$$

The three cases of p=0, p=1, and p>2 must be considered in the above expression. Considering p=0 leads to

$$\tilde{J}_o(z) = \frac{-2}{\pi z}\left[\cos^2(z)+\sin\left(z-\frac{\pi}{2}\right)\sin\left(z+\frac{\pi}{2}\right)\right] = 0.$$

Similarly, p=1 yields

$$\tilde{J}_1(z) = \frac{-2}{\pi z}\left[\cos\left(z+\frac{\pi}{2}\right)\cos\left(z-\frac{\pi}{2}\right)+\sin^2(z)\right] = 0$$

and p>2 yields

$$\tilde{J}_p(z) = \frac{-2}{\pi z}\left[\cos\left(z+\frac{\pi p}{2}\right)\cos\left(z-\frac{\pi p}{2}\right) + \sin\left(z-\frac{\pi p}{2}+\frac{\pi}{2}\right)\sin\left(z+\frac{\pi p}{2}-\frac{\pi}{2}\right)\right] = 0.$$

Thus, it may be concluded that for all l and m, $\tilde{J}_l(\lambda a)$ and $\tilde{J}_m(\lambda a)$ tend

asymptotically to zero for large values of λ; therefore, the integrand in spectral integral (4.34) approaches zero for large values of λ ($|_{\infty} \approx 0$) as was assumed in section 4.3. This renders the numerical integration convergent.

Similar manipulations may be practiced on inversion integral (4.35), which represents the matrix elements for the circumferential mode, leading to the same conclusions.

APPENDIX D

APPENDIX D

RESIDUE EVALUATIONS FOR SURFACE WAVE POLES

Evaluation of spectral integral (4.34) about the TM pole contour (C_{TM}), depicted in Figure 6, demonstrates the procedure used for all residue calculations for both spectral integrals (4.34) and (4.35). For convenience, spectral integral (4.34) is expressed as

$$B_{lm} = \int_0^{\infty} \left[F_1(\lambda) + \frac{F_2(\lambda)}{Z^e(\lambda)} \right] d\lambda$$

where

$$F_1(\lambda) = \frac{k_c^2 - \lambda^2}{Z^h(\lambda)} \lambda \tilde{J}_l(\lambda a) \tilde{J}_m(\lambda a)$$

$$F_2(\lambda) = \frac{\lambda^3 (N_{fc}^2 - 1) p_c}{Z^h(\lambda)} \tilde{J}_l(\lambda a) \tilde{J}_m(\lambda a).$$

Considering only the integration about the TM_{even} pole leads to evaluation of

$$I_{TM} = \int_{C_{TM}} F_1(\lambda)\, d\lambda + \int_{C_{TM}} \frac{F_2(\lambda)}{Z^e(\lambda)} d\lambda. \qquad \text{(D1)}$$

Since $F_1(\lambda)$ is everywhere analytic within and on C_{TM}, the first term in

expression (D1) yields no contribution. Further, assuming C_{TM} to be limitingly small and $F_2(\lambda)$ to be a slowly varying function of λ in the proximity of the pole, integral (D1) may be approximated as

$$I_{TM} \approx F_2(\lambda_p) \int_{C_{TM}} \frac{d\lambda}{Z^e(\lambda)}. \tag{D2}$$

Considering the leading terms in a Taylor series expansion of $Z^e(\lambda)$, given as

$$Z^e(\lambda) \approx Z^e(\lambda_p) + (\lambda - \lambda_p) \frac{\partial}{\partial\lambda} Z^e(\lambda)\Big|_{\lambda=\lambda_p}$$

(where the first term vanishes by definition), allows integral (D2) to become

$$I_{TM} \approx \frac{F_2(\lambda_p)}{Z^{e'}(\lambda_p)} \int_{C_{TM}} \frac{d\lambda}{\lambda - \lambda_p} \tag{D3}$$

where

$$Z^{e'}(\lambda_p) = \frac{\partial}{\partial\lambda} Z^e(\lambda)\Big|_{\lambda=\lambda_p}.$$

Considering the following local polar coordinates

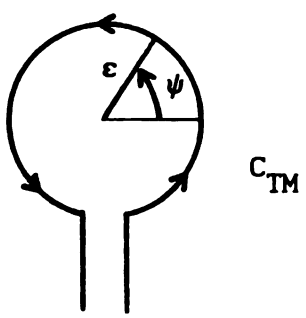

$$\lambda - \lambda_p = \varepsilon e^{j\psi}$$

$$d\lambda = j\varepsilon e^{j\psi} d\psi$$

allows integral (D3) to finally be evaluated as

$$I_{TM} = \frac{F_2(\lambda_p)}{Z^{e'}(\lambda_p)} \int_{-\frac{\pi}{2}}^{\frac{3\pi}{2}} j d\psi = 2\pi j \frac{F_2(\lambda_p)}{Z^{e'}(\lambda_p)}.$$

APPENDIX E

APPENDIX E

ANALYTIC REAL LINE INTEGRATION NEAR SURFACE WAVE POLES

When numerically evaluating spectral integrals (4.34) and (4.35), the real line integration (refer to Fig.6) in the neighborhood of the surface wave poles leads to potential numerical overflow problems. These complications arise because the pole values reside very near the real axis. To overcome this difficulty, the real line integration of spectral integrals (4.34) and (4.35) in the proximity of the poles may be analytically evaluated. Analytic evaluation of spectral integral (4.34) near the TM pole (expressed as $\lambda_p=\lambda_{pr}+j\lambda_{pi}$) illustrates the general procedure.

Considering only the real line integration and rearranging the integrand of integral (4.34) yields

$$I_{real} = -\int_0^{\infty} \left[F_1(\lambda) + \frac{F_2(\lambda)}{Z^e(\lambda)} \right] d\lambda \qquad \text{(E1)}$$

where

$$F_1(\lambda) = \frac{k_c^2 - \lambda^2}{Z^h(\lambda)} \lambda \tilde{J}_l(\lambda a) \tilde{J}_m(\lambda a)$$

$$F_2(\lambda) = \frac{\lambda^3 (N_{fc}^2 - 1) p_c}{Z^h(\lambda)} \tilde{J}_l(\lambda a) \tilde{J}_m(\lambda a).$$

By considering a small portion of the real line, with a width of 2ε centered at the real part of the pole, in expression (E1) leads to the evaluation of

$$I_p = -\int_{\varepsilon}^{\varepsilon} \left[F_1(\lambda) + \frac{F_2(\lambda)}{Z^e(\lambda)} \right] d\lambda.$$

Assuming F_1 and F_2 to be continuous and slowly varying in the region of interest leads to

$$I_p \approx -\left[2\varepsilon F_1(\lambda_{pr}) + F_2(\lambda_{pr}) \int_{\varepsilon}^{\varepsilon} \frac{d\lambda}{Z^e(\lambda)} \right].$$

Approximating $Z^e(\lambda)$ with the first two terms of a Taylor series expansion about λ_p as

$$Z^e(\lambda) \approx Z^e(\lambda_p) + (\lambda - \lambda_p) \frac{\partial}{\partial\lambda} Z^e(\lambda)\Big|_{\lambda=\lambda_p} \tag{E2}$$

permits I_p to be expressed as

$$I_p \approx -\left[2\varepsilon F_1(\lambda_{pr}) + \frac{F_2(\lambda_{pr})}{Z^{e'}(\lambda_p)} \int_{\varepsilon}^{\varepsilon} \frac{d\lambda}{\lambda - \lambda_p} \right] \tag{E3}$$

where the first term in expansion (E2) is zero by definition and

$$Z^{e'}(\lambda_p) = \frac{\partial}{\partial\lambda} Z^e(\lambda)\Big|_{\lambda=\lambda_p}.$$

The remaining integral in expression (E3) is evaluated as

$$\tilde{I} = \int_{-\varepsilon}^{\varepsilon} \frac{d\lambda}{\lambda - \lambda_p} = \int_{-\varepsilon}^{\varepsilon} \frac{d\lambda}{(\lambda-\lambda_{pr}) - j\lambda_{pi}}$$

$$= \ln\left(e^{j[\pm\pi - 2\tan^{-1}(\lambda_{pi}/\varepsilon)]}\right)$$

$$= j[(\pm\pi - 2\tan^{-1}(\lambda_{pi}/\varepsilon)]. \qquad \text{(E4)}$$

The proper choice of sign in expression (E2) is chosen to satisfy the branch cut of the ln function (negative real axis). Since $\lambda_{pi}>0$ and $\arg(\tilde{I})$ must reside between $+\pi$ and $-\pi$, the plus sign is chosen. Thus, I_p is evaluated as

$$I_p \approx -\left[2\varepsilon F_1(\lambda_{pr}) + \frac{F_2(\lambda_{pr})}{Z^{e'}(\lambda_p)} j[\pi - 2\tan^{-1}(\lambda_{pi}/\varepsilon)] \right].$$

LIST OF REFERENCES

[1] W.C. Chew and J.A. Kong, "Resonance of the axial-symmetric modes in microstrip disk resonators," *J. Math. Phys.*, vol. 21, no. 3, pp. 582-591, Nov. 1979.

[2] W.C. Chew and J.A. Kong, "Resonance of nonaxially symmetric modes in a circular microstrip disk," *J. Math. Phys.*, vol. 21, no. 10, pp. 2590-2598, Apr. 1980.

[3] Kiyomichi Araki and Tatsuo Itoh, "Hankel Transform Domain Analysis of Open Circular Microstrip Radiating Structures," *IEEE Trans. Antennas Propogat.*, vol. AP-29, no. 1, pp. 84-89, Jan. 1981.

[4] J.S. Bagby, D.P. Nyquist, and B.C. Drachman, "Integral formulation for analysis of integrated dielectric waveguides," *IEEE MTT-S Trans.*, vol 33, no. 10, pp. 906-915, Oct. 1985.

[5] R.E. Collin, Field Theory of Guided Waves, New York: Mcgraw Hill, 1960.

[6] J.S. Bagby and D.P. Nyquist, "Dyadic Green's functions for integrated electronic and optical circuits," *IEEE MTT-S Trans.*, vol. 35, no. 2, pp. 206-210, Feb 1987.

[7] A.D. Yaghjian, "Electric dyadic Green's function in the source region," *Proc. IEEE*, vol. 68, no. 2, pp. 248-263, Feb. 1980.

[8] M.S. Viola and D.P. Nyquist, "An observation on the Sommerfeld integral representation of the electric dyadic Green's function for layered media," *IEEE MTT-S Trans.*, vol. 36, no. 8, pp. 1289-1292, Aug. 1988.

[9] D.P. Nyquist, to appear in the proceedings of the URSI Triennial Electromagnetic Theory Symposium, Stockholm, Sweden, August 14-17, 1989.

[10] M. Abramowitz and I.A. Stegun, Handbook of Mathematical Functions, New York: Dover Publications, Inc., 1972.

[11] S. Ramo, J.R. Whinnery, and T. Van Duzer, Fields And Waves in Communication Electronics, New York: John Wiley & Sons, 1984.

[12] M. Blischke, Broadband Analysis of Radiating, Receiving and Scattering Characteristics of Microstrip Antennas and Arrays, Ph.d dissertation, Michigan State University, 1989.

[13] I.S. Gradshteyn and I.M. Ryzhik, Table of Integrals, Series, and Products, Orlando: Academic Press, 1980.

[14] W.R. Lepage, Complex Variables and the Laplace Transform for Engineers, New York: Dover Publications, 1961.

[15] Weng Cho Chew, "Resonance Frequency of a Rectangular Microstrip Patch," *IEEE Trans. Antennas Propogat.*, vol. 36, no. 8, Aug. 1988.

[16] Y.T. Lo, D. Solomon, and W.F. Richards, "Theory and Experiment on Microstrip Antennas" *IEEE Trans. Antennas Propagat.*, AP-27 (1979), 137-46.